https://doi.org/10.1016/j.nanoen.2020.105437

High Energy X-ray Radiation Sensitive Scintillating Materials for Medical Imaging, Cancer Diagnosis and Therapy

Lu Lu[1], Mingzi Sun[1], Qiuyang Lu[1], Tong Wu[1], and Bolong Huang[1]*

[1]*Department of Applied Biology and Chemical Technology, The Hong Kong Polytechnic University, Hung Hom, Kowloon, Hong Kong SAR, China*

*E-mail: bhuang@polyu.edu.hk

Abstract

X-rays are widely adopted in cancer radiotherapy and clinical diagnosis devices for photodynamic therapy (PDT) and medical radiography. The sole utilization of X-ray irradiation for tumor therapy results in insufficient radiation energy deposition of initial X-ray photon energy owing to the low attenuation coefficient for X-ray in organisms, generating overdose ionizing radiation with great lethality to normal cells. Recent achievements in materials engineering and nanotechnology accelerate the exploiting of X-ray excited scintillating systems. These cancer-site targeting scintillators are able to absorb and convert X-rays into visible light emissions, which relieves the risk of overdose X-ray exposure. In medical imaging, X-ray radiation is ideal for the excitation of scintillating materials in clinical diagnostic and therapeutic applications owing to its extraordinary penetration power in tissues and organs. In this review, we will summarize the corresponding X-ray excited scintillating mechanisms and related material advances in detail to offer an overview of novel scintillating materials for medical imaging and tumor-associated PDT.

Keywords: X-ray Radiation; Scintillating Materials; Bio-image; Cancer Diagnose; Photodynamic Therapy

1. Introduction

The invisible high energy radiation rays (X- α-, β-, and γ-rays) were first detected by scientists in the 1890s on account of their capacity to excite phosphors like $K_2Pt(CN)_4$.[1] The strong penetrating power of X-rays (0.01-10 nm)/γ-rays (<0.01 nm) enables them to clearly demonstrate the inside structure of the scanned condensed objects for non-destructive security inspection and medical imaging.[2-4] After ionizing the subjects by interaction with the atomic electrons, X-ray/γ-ray can export accurate inside retrieval information of the inspected objects through the difference in radiant properties (phase, direction, dose rate/photon intensity, and wavelength).[2] The radiation penetrates the subjects and its attenuation is detected and analyzed.[5-6] The image contrast derives from the variable signal detected in the absorption of radiation preventing the capacity of various organs/subjects to the radiation. However, these rays can hardly be sensed by ordinary photographic substrates, so researchers are dedicated to exploring scintillating materials that are able to absorb these rays efficiently and convert the absorbed X-ray radiation into photon radiation emitted within the visible light range. Then the visible emission could be detected and converted into electric signals by photoelectric detectors for further data analysis.[7-8]

Scintillators are a series of particular energy conversion materials that can absorb and convert X-rays/γ-rays radiations into the visible light region. In early X-ray based imaging, conventional photographic films were found rather inefficient; to cooperate with the photographic-film based detectors efficiently, the scintillators were therefore employed to convert the invisible radiation (X-rays/γ-rays) into visible-light range.[9] Though scintillators are not able to achieve X-ray medical imaging directly, they can decrease the radiation dose required for imaging. During the past several decades, the most widely studied conventional scintillators are Bi, Ce, Eu, Tl, Pb, W, etc. contained inorganic materials.[10] Some of these elements are usually used as dopant elements (Bi,[11-12] Ce,[13-16] Eu[17] and Tl[18-19]), and some are generally adopted as host materials (Bi[20-22], Pb[23-24] and W[12]). These metal atoms share a common characteristic of the relatively high atomic numbers (high-Z), which accounts for the high stopping power and good scintillation performance.[10] The functional heavy elements based scintillating materials contribute a lot to the fields of nuclear energy, non-destructive security inspection, industrial detection as well as clinical imaging/therapy.[25-27] Exploring novel X-rays/γ-rays induced scintillators with tunable luminescence performance is a core research target toward specific fields. Due to the relatively low density of chemical constituents, organic scintillating materials still exhibit inherent weakness for the detection of high-energy radiations.[28] Heavy metal ions are substantially adopted to construct inorganic scintillating materials based detectors because of their high energy resolution and energy-conversion efficiency.[29]

$CaWO_4$, NaI: $Tl^{+,}$ and $Bi_4Ge_3O_{12}$ are three popular types of scintillators adopted in imaging applications. The $CaWO_4$ was adopted as X-ray phosphor for about 75 years since the year 1896.[30] This crystal was able to convert the absorbed X-ray radiation into blue light, which enabled X-rays based medical imaging for the skeleton and organs of humans. NaI: Tl^+ was served as a scintillator in γ-imager for the detection of γ-rays for several decades.[31] $Bi_4Ge_3O_{12}$ (BGO) was first discovered as an X-ray detector by Weber in the year 1973, and it was also found absorption in other categories of radiations in post studies. BGO was ever utilized as γ-rays based positron emission tomography (PET) in crystalline form for medical diagnosis.[1]

After the development of more than a century,[32] the investigations on X-ray radiation excited scintillating materials are still promising since the performances of ionizing radiation devices are upgrading, and novel technologies on synthesizing related functional nanomaterials have also been improved. The exploration of novel scintillators is oriented to specific requirements of radiation detection in diverse application fields. Most studies concentrate on improving the detection efficiency of the typical scintillators by crystal engineering.[29] Apart from the constituents, attempts on transforming the existing scintillators into different forms (such as bulk single-crystal, nanoparticle, fiber, film, etc.) have also exhibited distinct progress in some scintillating systems.[7, 29] Metamaterials and hybrids are also a new tendency.[33] Doping is another mature technique for material modification, which provides many successful cases in tuning the luminescent performance.[34-36] Since bulk single-crystal scintillating materials are difficult and expensive to be synthesized,[37-38] there is little flexibility in regulating their chemical constituents or searching for alternative doping elements and crystal shapes. The hygroscopic effect, poor ruggedness, as well as limited design flexibility, impose extra constraints on bulk scintillating materials. The engineering of materials in nanoscale with tunable scintillating performance is an alternative that provides new solutions to the restrictions mentioned above.[39-41] Compared to single crystals, colloidal nanocrystals are relatively low cost, easy in synthesis technique and flexible in performance modification.[42]

In biomedical applications, X-ray imaging has been the most widely used clinic tool for medical imaging and diagnosis, which aims to visualize the organs in a non- or minimally invasive way. To supply a more accurate diagnosis and clinic information, novel X-ray sensitive scintillators are highly needed to allow the in-vivo molecular-imaging-based investigations of biochemical pathways. Although many X-ray scintillators have been proposed and studied in previous work, many challenges still exist to be overcome in the future such as the complicated synthesis method, the hygroscopicity of the inorganic scintillating materials, the anisotropic scintillation of organic crystals, the unsatisfying light yield. [43-44] Therefore, discovering more novel X-ray sensitive scintillating materials is significant for broad medical applications.

This paper concentrates first on the rising demands of novel scintillating materials. Special attention is paid to the requirements in the medical imaging and photodynamic therapy field. We will introduce recent achievements in co-doping rare-earth scintillating systems and heavy-metal based perovskite-like nanoscintillators. Since all these developments have a close connection with the knowledge of the scintillating principles, it is also crucial to elaborate on the recent progress on luminescent mechanisms as well.

2. Development History of Scintillating Materials

Perovskite-structured materials are research hotspots in recent decades and have been investigated intensively due to the unique optical and electrical performance benefiting from their variable constituents and structures for wide applications.[45-48] The earliest identified perovskite is $CaTiO_3$ (ABO_3), which was derived into diverse compositions later including ABX_3, A_2BX_6, $A_2BB'X_6$, $A_3B_2X_9$, A_4BX_6, etc.. In these structures, both A and B are cations, and the radius of A is generally larger B. The diverse formula forms and variable structures endow perovskite-like materials with tunable properties for broad applications.[48-51] Due to their unique photoelectric

properties, luminescent perovskite-like materials have been widely applied in the areas of digital displays, photoelectric sensors, illumination, and medical imaging and so on.[52-56]

Modern X-/γ-ray perovskite detectors mainly depend on two types of energy conversion mechanisms. In photon to current conversion mechanism, the semiconductor can directly convert the incident radiation into the photoelectric current.[57-59] For scintillator based detector, X-ray is converted into UV/Vis photon *via* a down-conversion mechanism, and the scintillating matter is integrated into a sensitive detector working at relatively low photon energy.[60] By contrast to semiconductor based detectors, the suffering of limited carrier diffusion length of absorption material can be avoided in X-ray scintillating materials.[61-62] With a scintillation response time in sub-ns range, phenethyl-ammonium lead bromide (PhE-$PbBr_4$) thin-film based scintillating materials have been previously studied by X-ray[63] and proton[64] excitation. Limited by the film thickness of 200 μm, the detection efficiency of PhE-$PbBr_4$ is only 5%-6% in 60 keV X-ray radiation.[64] Through combining the fast response toward X-rays with big absorption cross-section stemming from the thickness and relatively high mass density, single-crystal perovskite-like scintillating materials are hence developed to enhance the detection efficiency under keV X-/γ-ray radiation.[23]

Lead-halide perovskite single crystals are popular scintillating materials, exhibiting short absorption length as well as high detection efficiency to X-rays.[23] Integrated with large absorption cross-section originating in large thickness and high mass density, they exhibit fast response to X-ray excitation.[23] However, single-crystal perovskites can only exhibit satisfactory scintillating performance at relatively lower temperature conditions (under 130K),[65] and they are quite sensitive to air and humidity.[66] With the upgrading of nanotechnology, researchers have made attempts to downscale the perovskite size into the nano-scale, to further enhance their scintillation performance.[45, 67-68] Compared to bulk perovskites, perovskites in nano-regime (PNMs, including nanoparticles, nanowires, nanofilms, and so on) demonstrate a series of superiorities. PNMs have better process-ability for the manufacture of functional thin films and flexible devices,[68] and PNMs also feature rich and tunable facets as well as active sites for catalysis.[69] In addition, taking advantage of the quantum effect and small-size effect, PNMs are endowed with superior optical and electromagnetic properties.[70] However, it should be noted that the requirement of some kind of suspension of nanoparticles may decrease the effective density and stopping power.

Due to their distinctive electronic structures, the halide perovskite nanocrystals/quantum dots (QDs) have high emissive triplet states in excited states, resulting in a high radiation coefficient.[71-72] Owing to the quantum constraint effect and the increase of wave-function overlapping in both electrons and holes, the spatial distribution of the excitons produced by X-rays in recombination centers and can be restricted within the Bohr radius of the nanocrystals /QDs. The scintillating properties are tunable in visible region because of their abundant electronic states and the adjustable bandgap value. They also have high detection efficiency and relatively lower reabsorption to X-rays.[73-75] Nevertheless, pristine perovskites have some intrinsic deficiency. For example, some halide PNMs have limited adaptability for both optical and electrical performances, and they exhibit poor stability for light, heat, oxygen, humidity and have obvious aggregation and phase transition. [76-77] Some oxide

PNMs exhibit unsatisfactory catalytic and photo-electro-magnetic performances.[46, 51, 78] Researchers have made attempts to add external doping ions into PNMs to conquer these drawbacks.[47, 68] Rare earth (RE) elements, regarded as 'the vitamins of modern industry', have been widely adopted as dopants or constituents in host lattice to regulate the specific physical or chemical characters for target applications.[79-80]

The image resolution can be enhanced by considering the travel distance of γ-rays, so time-of-flight positron emission tomography (TOF-PET) is an upgraded technology for traditional PET.[81] TOF-PET requires a considerably fast scintillation response. The inorganic scintillators applied in PET such as LSO:Ce and GSO:Ce have a high density of 7.0 g/cm^3 and high LY of more than 10000 photons/MeV. However, they have a response time of over 40 ns.[82] Another potential candidate for high-quality imaging is organic-inorganic hybrid scintillators such as BC452 that have a quite short decay time of several nanoseconds with a high LY of 10000 photons/MeV but the organic-inorganic hybrid scintillator BC452 still suffers from the low density of 1.0 g/cm^3 and low chemical stability.[83]

The effects of spatial dimensional forms on perovskite scintillators have also been tested in previous researches, in which comparative studies on the scintillation performances of two dimensional (2D) and three dimensional (3D) perovskite-structured single crystals with narrow bandgap have been thoroughly conducted. The 2D perovskite single crystals have greater resistance against thermal quenching owing to the large exciton binding energy caused by the charge confinement in their inorganic layers.[83] These research results validate the outstanding properties of metal-halide perovskite scintillators for X-/γ-ray detection and indicate the superiority of 2D perovskite scintillating crystals with large exciton binding energy for X-ray scintillation with high LY. The 2D Pb-halide perovskite scintillators can show quite fast response time in TOF-PET.[84] The small bandgap value is also beneficial because the limit of the corresponding scintillator's LY in theory is inversely proportional to the bandgap value. However, due to the self-absorption effect induced by the minimum Stokes shift of exciton emission, the energy resolution as well as the LY of 2D perovskite scintillating materials are declined, resulting in longer emission duration time.[23, 85]

3. Criteria of Scintillating Materials in Applications

Nowadays, scintillators are widely applied in many detection materials in various fields, particularly in nuclear security[86], medical diagnosis[73, 87-88], and photodynamic therapy[89-90]. Perfect scintillators ought to demonstrate the following properties: high photo quantum yield, quick response time, good radiation preventing capability, flexible radiation, hygroscopic rigidity as well as high energy resolution.[91] Whereas, the demands in these performance parameters strongly depend upon specific application contexts. Most of the scintillator-based instruments were developed based on three main parameters: density, spatial resolution, and time response speed. As for homeland security, it demands widely deployed detecting systems for the spectroscopy of γ-rays. So, the decay time is not the key point to be considered but the growing demands on energy resolution emerged. The crucial requirement on high energy resolution results in the developments of rear-earth ions doped halide scintillators such as $LaBr_3$: Ce^{3+} and SrI_2: Eu^{2+}.[92-93] Whereas, the requirements of radiation detectors employed in X-ray or nuclear medical imaging instruments are high detection efficiency and spatial resolution. Relatively short decay time, weak afterglow emission, and high stopping power are the present demands on scintillators. In the case of single-

photon emission computed tomography (SPECT) imaging, the easy growth technique of large flat panels have made NaI (Tl) a dominating material.[94] As for PET scanners, high stopping power and fast response are both required and the researches mainly focus on LSO: Ce and LYSO: Ce.[95]

The selection of scintillating materials depends on the requirements of specific application fields. The main parameters that influence the selection of a certain scintillating material are indicated as follows: [60, 96]

1) Absorption efficiency: for photon radiation, this parameter characterizes the efficiency that a scintillator can absorb the radiation energy in the conversion process. High-density and high-Z scintillators are prior choices for X-/γ-ray excitation. As for the radioactive particle, it refers to stopping power, determining the efficiency that a scintillator absorbs the kinetic energy of the radioactive particles.
2) Detection efficiency: the detection efficiency is the ratio of X-ray/γ-ray photons absorbed in the detector divided by the number of incident photons (internal detection efficiency).
3) Light yield (LY): absolute LY refers to the rate of the total energy of emitted photons to the energy deposited by the incoming radiation in the scintillator, and it can be characterized by the number of emitted photons per unit (photons/MeV) absorbed by scintillating material.[97] The LY hinges on the quantity of electron-hole pairs generated in the ionization tracks, which is closely related to the value of bandgap(E_g).[98] It can be calculated by $LY=10^6 \cdot SQ/(\beta E_g)$, where S refers to the transportation efficiency of charge carriers, Q refers to the luminescent quantum efficiency and β is a constant. However, caused by the internal scattering and reabsorption, losses of photons will occur during the propagation to the detector. Thus, technical LY might be lower than the calculated value.
4) Response time: the duration time for the scintillating materials to emit photons in the UV/Vis range after the absorption of radiation energy. Fast response time or short decay time is vital for scintillation based detection where timing is involved. Persistent luminescence (PL) induced by additional electrons/holes trapping process is disadvantageous for scintillation applications. The quenching process will shorten the decay time but result in a decrease of LY.
5) Energy resolution: the ratio of the full width at half maximum of a given energy peak to the peak position. This parameter is very important for the spectroscopic characterization of incident radiation, and it exhibits the detector performance on distinguishing the γ-ray spectrum in close energies. The intrinsic energy resolution is primarily affected by the non-proportional response. Whereas the defects like the heterogeneities of the crystal will give rise to local variation in light output, and inhomogeneous reflectivity also influences energy resolution.[99]
6) Radiation hardness: it reflects the scintillation ability of the material not to degrade remarkably when exposed under high-energy ionizing/particle irradiation. Although radiation damage may have little relationship with the detection process in common imaging applications, it is an important parameter in high-energy physics researches.[100] Radiation hardening is used to improve the resistance of damage or malfunction induced by high-energy radiation for the construction of electronic detecting devices.[101] Due to its radiation hardness and satisfactory response in the radiation triggered luminescent process,[102-103] alumina can serve as a good scintillator in highly irradiating conditions like the nuclear reactor.

7) Emission wavelength: the emission wavelength as well as LY will determine the optimal photodetector to be adopted.[100] To eliminate post-scintillation losses, the optimal detecting sensitivity range of photodetector should overlap the emission spectrum of the scintillator. To align their emission wavelength with the available detectors, some scintillators might need to be regulated by materials engineering.
8) Stability: this parameter determines the lifetime that a material can serve as a scintillator with satisfying scintillating performance before it has to be replaced. Chemical stability reflects the intrinsic stability of the scintillator such as self-life while radiation stability reflects radiation hardness.
9) Proportionality: the scintillating response should be linear under incoming radiation, and this property will affect the distinguishing capability of intensity. With computational correction techniques, it is possible to amend a non-linear response. However, it is advantageous for the scintillating material to have a linear response, especially within the sensitivity scope of the photodetector.

The following figures of merit for image resolution hinge upon the interaction between scintillating material and detector rather than the intrinsic features of scintillators.
1) Spatial resolution: it is a parameter for characterizing the image sharpness, exhibiting the contrast and the amount of blurs over a certain range of spatial frequencies. and it can be quantitatively evaluated via the modulation transfer function (MTF). [104]
2) Imaging performance: it reflects the effectiveness of X-ray imaging for generating an image with a relatively high signal-to-noise ratio (SNR) in the optimal photodetector. Unlike modulation transfer functions, the SNR is the detective quantum efficiency, integrating the effects of image contrast related signal and noise, which is usually expressed as a function of spatial frequency.

In particular, for medical applications such as X-ray imaging, the most important criteria are summarized below [105].
1) High absorption coefficient for the X-ray, which is crucial for achieving a reasonable quality of imaging with the lowest patient dose exposure.
2) High light output is significant to reduce the noise signal during the X-ray imaging.
3) Decay time should be in the range to match the CT scanners in ≥10 kHz range.
4) The most important constraint for X-ray imaging is the absence of afterglow, which causes sickle artifacts in the imaging.
5) Low temperature dependence of the LY.

Meanwhile, for PET or SPECT, there are several requirements of the X-ray scintillating materials to guarantee the high image signal to noise ratio.
1) The high detector sensitivity.
2) The high spatial resolution.
3) The high energy resolution.
4) The high temporal resolution.

The abovementioned four parameters are key to the detection chain of PET and SPECT. To satisfy these requirements, the high light yield is needed to improve the energy resolution. The higher energy resolution is also beneficial to improve the sensitivity and spatial resolution. Good image contrast is attributed to higher sensitivity. Therefore, to achieve the selection or search of a novel scintillator for a specific scintillating application, these fundamental parameters, and criteria, especially the absorption

efficiency, LY, emission wavelength, and stability, need to be carefully considered.

4. Scintillating Mechanism Investigations

4.1 Defect-related Intrinsic Scintillating Mechanism

Nanophotonic energy storage (NPES) materials have been identified as potential scintillators, which accept a broad spectrum scaling from X-ray to near-infrared (NIR).[106-109] Persistent luminescence (PL) is a typical example of the NPES effect.[110] These materials usually possess a class of the slow-release trapped charge carriers towards recombination after removing the external excitation energy. To achieve the target scintillation performance, the activators and trapping-centers will be the most determining factors because they dominate the energy level positions of recombination centers and trapping depths, respectively. The activators are where the electrons and holes recombine after excitation for output emission, where the wavelength is determined by the energy difference between electron initial and final state. Thus, the excitation energy can be stored through the localization of excited electrons at trapping-centers. Meanwhile, the energy can be gradually released by thermal or photostimulations to realize the emission based on electron-hole recombination. For such scintillation materials, their performance regarding the output intensity and duration time of the NPES effect is controlled by the concentrations and depths of trap centers, which are usually considered to be intrinsic defects.

For the scintillation materials as $NaREF_4$ (RE=Rare earth ions), our group identified that the level-matching induced surface resonant quantum tunneling (LM-SRQT) effect has been the key factor to control and modulate the surface electronic process for efficient NPES effect.[110] Specifically, surface alkaline ions are essential for stabilizing both the surface and in-bulk photo-generated local micro-electric-fields (**Figure 1a-1c**). Through the hole and electron self-trapping, we further confirm that surface states are able to produce localized electronic and hole states (Figure 1d-1f). The surface inhomogeneous electronic states of nanoparticles are originated from the defective F- and Y-sites or those tri-positively charged lanthanide ion sites. Further volume-to-ratio calculation confirms the existence of surface defect states regardless of the stoichiometry ratios (Figure 1g). To screen out the NPES nanomaterials, our group has proposed that the intrinsic level-matching induced surface resonant quantum tunneling (LM-SRQT) effect should be the key driving force to accomplish the recombination of charge carriers. The surface defects states induced by the surface non-crystallization enables the connection of the energy conversion among the same type of defect sites through the transient time-scaled excitations and long-lifetime localizations (Figure 1h). Eliminating the persistent luminescence will enable the application of $NaYF_4$ in a CT scan. The persistent luminescence is expected to be restrained by realizing the nonradiative recombination of de-trapped holes/electrons at the luminescent center through selecting suitable doping strategies.[111] Through unraveling the surface defect states, our previous work offers a good reference to guide the researchers to select potential doping ions to suppress the afterglow emission.

4.2 Mechanism of the Scintillating Process

The scintillating process mainly includes three main stages: (I) conversion, (II) energy transfer (ET) and charge carrier migration and (III) scintillation.[98, 112-116] In the first stage of scintillation, the energy conversion process occurs just follows the interaction between the matter and incoming photons/ionizing particles. Highly energetic charge carriers are generated after the irradiation energy is absorbed by the

scintillating material. The corresponding energy absorption mechanism hinges on the specific sort of radiation energy involved. As for X-/γ-rays, it can be expressed by the formula of $I/I_0 = e^{-\mu d}$, where I_0 and I refer to the incoming and transmitted radiation intensity, respectively. The μ refers to the value of the linear absorption coefficient and d refers to material thickness. Three sorts of interactions between radiation and scintillator are involved in contributing to conversion: photoelectric absorption,[117] Compton scattering[118] as well as pair formation (hυ>1022 keV).[119] These processes exhibit different absorption coefficients that largely hinges on the Z values of lattice atoms and the energy of incident radiation. The absorbed radiation energy will give rise to the creating of highly energetic charge carriers in the scintillator lattice.[115] The hot electrons appearing in the crystal further interact with other particles or pseudo-particles such as electrons, phonons and plasmons, resulting in the avalanche occurrence of secondary electrons and holes. This process continues until the hot electrons and secondary electron-hole pairs lack sufficient energy to ionize the ions in scintillator lattice. The generated abundant energetic electrons/holes will then experience energy dissipation by interactions with phonons, which is also called thermalization process.

The second stage mainly involves the process of electrons and holes migration to the luminescent centers, which has a significant influence on the energy losses, electrons/holes trapping, and timing performances. Previous reports have proposed several models to explain both the delay of luminescence and losses of energy by non-radiative recombination procedures.[96, 116] The existence of imperfections in scintillator lattice is the main cause of the losses, mostly arising from native point defects such as vacancy and interstitial, grain boundaries, impurities or dopants, interfacial and surface states. Besides native imperfections, the interaction between scintillating matter and radiation also contributes to the defect formation, especially the Frenkel defects, created by the atom out of its original lattice position and stabilizes in the lattice interstitial, leaving a vacancy behind.[120-121] As a result, the migrating electrons/holes can be captured and stored in these trap states, mostly in the defect states of vacancy. Affected by temperature, the trapped charge carriers will be de-trapped and further migrate by phonon aided transportation.[122] The charge carriers also migrate from the de-localized conduction band (CB) to more energetically preferable localized energy states by the coupling with phonon, resulting in slower migration of polarons. The transport state of scintillation is remarkably affected by the material manufacture procedure.[123] Therefore, the optimization of crystal growth conditions and modifications of material morphology are able to avoid the formation of defects in the lattice, which enhances the mobility of electrons/holes and then shortens the luminescent delay and non-radiative losses.

In the last stage, the charge carriers are captured *via* potential transition paths through emitting centers (usually impurity/dopant ions in the lattice) and promoted to excited states. Following the selection rules, electron-hole pairs then have radiative recombination and generate fluorescence emission in the UV/Vis region. The mechanism of electron-hole pairs recombination in emitting centers for light emission has been well described in the previous report.[124] In the case of fast emission, it is crucial to choose the recombination center exhibiting electric dipole allowed transitions, like the widely adopted $4f^{n-1}5d$-$4f^{n}$ transition in lanthanide ions. If the transitions are not electric dipole allowed, the electrons and holes have to experience additional procedures,[96] resulting in the delay of emission, which significantly lowers the

efficiency for fast-timing scintillation applications. Thus, besides referring conversion and energy transfer efficiency, the ions/molecules of the scintillator material are expected to be selected with allowed transitions for highly efficient radiative recombination in specific applications requiring fast decay time.

4.3 The Scintillating Mechanism of the Doped Lanthanides Based Compounds

Inorganic scintillating materials have been instigated extensively, the general principles of scintillation can be classified into two sorts: intrinsic patterns or extrinsic patterns (**Scheme 1**).[125] For intrinsic ones, the light emission is in association with the de-excitation process in which the electrons directly transit from the conduction band (CB) to the valence band (VB). The widely utilized scintillating materials BaF_2 and BGO are typical intrinsic scintillators. But this scintillation case is comparatively rare because the self-quenching process is very likely to occur when the ionic strength increases.[91] As for the extrinsic ones, it depends on external dopants to act as the sensitizer, which induces new doping energy levels emerging within the bandgap of the host lattice. Thus, because of the narrower electron transition gap, the sensitized extrinsic scintillators generally exhibit relatively longer emission wavelength than corresponding intrinsic counterparts. The majority of doped inorganic scintillating materials are in the extrinsic type, including CsI: Tl^+, SrI_2: Eu^{2+}, $LaBr_3$: Ce^{3+}, Cs_2LiYCl_6: Ce^{3+} and so on.[29, 31, 125] The luminescent performance of extrinsic scintillating materials such as light-yield, spectral range, Stokes-shift, and decay time can be systematically adjusted by bandgap engineering and modification of the coordination circumstance around the photoactive ions.[10, 126-127]

The principle of the doped lanthanides-based scintillation systems for X-ray medical imaging includes a transport process of electrons and holes. The migrating charge carriers in CB and VB must jump across the energy gap in their transition path to reach the recombination/luminescence center. Thus, the atomistic perfection of the crystal lattice becomes the major consideration for manufacturing the scintillating materials. However, it is a fact that the native point defects can hardly be avoided in single-crystal host lattice, mostly vacancy defects, which results in defect trap states appearing within the bandgap. Other types of lattice disorders such as the accidentally introduced impurities as well as the extended lattice dislocations and flaws can also generate electron/hole traps. Since optimization of synthesis technique cannot completely diminish these defects, other attempts have been made to modify the scintillating properties oriented to specific utilization. Introducing co-dopant ions into the host lattice is a kind of mature technology for lattice modulation.[128-129]

5. Scintillating Materials for X-ray Induced Medical Imaging

The boost in the application of high radiation dose based diagnose like computed tomography (CT) scans cannot avoid the hidden harm caused by radiation complications. High dose X-ray imaging raises the risk of suffering malignant tumors to the tester later in life, which is caused by the DNA damaging and the protooncogene activation via ionizing radiation.[130] For instance, the radiation dose received from a single chest CT is equivalent to the natural irradiation dose accumulated in two years.[130] It has been previously reported that the patients will suffer a high risk of the radiation-induced malignant tumors if the dose is above 100 mSv and an estimation of 2% of the cancers has a close connection with high dose radiation suffered during CT scan.[130] The high radiation dose required for CT scan mainly arises from the low

sensitivity of current detectors. Therefore, constructing a high-sensitivity detecting system for a CT scan is urgently needed.

It is a fact that CT detectors can achieve a detection efficiency of nearly 100%. It is possible for the detectors to absorb almost all the incoming X-ray photons with an energy of 110 keV. This goal can be easily achieved under low energy X-ray irradiation because of the relatively low penetrating power, and it just needs several ms to stop all the incident X-ray photons. However, the conundrum for CT detectors is caused by very high fluxes of X-ray radiation and the operation mode applied for such high intensities. Most of the CT systems are operated under current mode which suffers from the quite low signal-to-noise (S/N) ratio. The noise magnitude determines the smallest photo intensity that the radiation detector can measure. In addition to the increase of the signal intensity, restraining the background noise is also very crucial for obtaining a higher S/N ratio for many sorts of sensors.[131-133] The noise magnitude of a detector is mainly dominated by the dark current, although other kinds of noise also exist. The S/N ratio can be improved a lot in photon-counting mode, but the commonly used detectors (scintillators and photodetectors) cannot handle such high counting rates. Thus, developing fast, but very low light yield scintillators might be required for the photon-counting mode. Besides the S/N ratio, some other parameters such as spatial resolution, response time, proportionality and stability are also very crucial for obtaining high-quality X-ray images.[2]

5.1 Heavy Elements Enhanced Radiation Effects

Elements with the high atomic number (high-Z) are acknowledged to have great potential to serve as the radiosensitizers for X-ray based medical imaging.[134] Under the X-ray radiation, high-Z elements have larger photoabsorption cross-section.[135] The photoelectric effect can be confirmed since the materials (metal or non-metal) will emit photoelectrons when exposed under the photoirradiation. When irradiated with high-energy X-rays/γ-rays, heavy atoms generate a cascade of low-energy Auger-electrons, which boost the radiation dose for localized tumor therapy. Another approach to enhance the effective radiation dose is to employ nanoparticle-assisted radiation therapy.[136] This enhancement is related to the size and component of particles, loading capacity into cells, and irradiation energy. When exposed under X-rays radiation, the irradiance particles: scattered X-ray photons, fluorescent-photons, Auger-electrons as well as Compton-electrons are related to tumor radiotherapy. Additionally, the fluorescent emitters from the high-Z atoms heated by X-rays are very useful for cell imaging and photodynamic therapy.

5.2 Lanthanides Based Scintillating Systems

Lanthanides are high-Z elements with proper electronic energy states. The earliest rare-earth doped scintillators (LaF_3: Ce^{3+}, Pr^{3+}, Nd^{3+} [137] and YAG[138]) were reported in the late 1980s. Experienced development for several decades, the rare-earth doped scintillating systems have already offered satisfactory scintillating properties.[139] Pure CaI_2 has a very low density and low cross-section for photoelectric effect interaction, which limits its applications for γ-ray spectroscopy. Meanwhile, LuI_3 has been found very brittle and almost impossible to grow single crystals, reducing their potential as the scintillator. Recently, the rare-earth ions doped scintillating systems of CaI_2: Eu^{2+} [140] and LuI_3: Ce^{3+} [16] achieve the light output of more than 100,000 photons per MeV. Sr^{2+}, Ca^{2+} co-doped $LaBr_3$: Ce^{3+} system exhibit an ultrahigh energy-resolution of 2%,[129] while Ce^{3+} doped $PrBr_3$[141] and Nd^{3+} doped LaF_3[137] have an extremely

short scintillating decay time of 6 ns. These materials emit photons in the ultraviolet, visible, or near-infrared range when excited by X-rays/γ-rays, so they are treated as potential scintillating materials for medical imaging.[142] Lanthanides based nanoparticles (i.e. Eu^{2+} doped BaFBr, Tb^{3+} doped LaF_3, and Ce^{3+} doped LaF_3) are reported to have persistent luminescence (PL) after exposed to X-ray radiation.[143] The thermal quenching effect is likely to give rise to the low light yield, which should be suppressed for the room-temperature scintillators. Interestingly, the PL duration will increase when detected at higher in-vivo temperature. The doped Gd_2O_2S (GOS): Pr, Ce^{3+}, F^- system is a successful example[111], which eliminates the afterglow emission and extends its further application in X-ray computed tomography (CT) based medical imaging. The afterglow emission is suppressed mainly because the nonradiative recombination of de-trapped holes/electrons at the co-doping energy levels limits the delayed recombination process at the luminescent centers. Great efforts have been devoted to the developments of rare-earth halides owing to their remarkable light yield and energy resolution. However, these material family all shows the relatively low density and a high hygroscopicity, which restrict their applications in the PET scanners. In the application of scintigraphy camera, rare-earth halides have shown competitive performances to the commercial materials.

5.2.1 Applications of Lanthanides Based Scintillating Systems

In successful lanthanide-based scintillating systems for CT imaging, versatile Tb^{3+} doped LaF_3-Rose Bengal (RB) scintillators were coated with a homogenous silica layer for the pathologic diagnosis of cancer.[144] The shell-thickness of the coated layer is controllable and the substrates form covalently bound toward RB. This nanocomposite has a uniform size, good biocompatibility, high colloidal stability, and photostability. And the X-ray damping was detected, and the in vivo X-ray bio-imaging was conducted on the tumor of the mouse. After the nano-scintillator has been injected into the tumor site, the signal intensity enhances considerably. As indicated in **Figure 2a-c**, the measured X-ray attenuation power surpasses the commercial CT contrast instrument (Ultravist® 300), which makes it an ideal CT contrast agent for deep-tumor diagnosis. And the Sc NPs-RB nanoscintillator also exhibit faster decay time (Figure 2d). Though promising in CT imaging, more experiments are still required to further verify the photodynamic therapeutic efficacy of the Tb^{3+} doped LaF_3-RB scintillating material by X-ray activation. Exploring multiplexed scintillators has become a research hotspot for the construction of dual model imaging devices.

Due to the combined luminescent properties, X-rays excited and re-excited nanoscintillators have attracted extensive research interests in biological applications especially in the medical imaging field. For instance, under X-ray radiation, Co and Cu codoped ZnS Nano-scintillators have a wide emission band peaked at about 510 nm, while the afterglow emission centered at 546 nm. This spectrum feature suggests that the existence of the two different emission process.[145] Then the photo-activator tetrabromorhodamine-123 (TBrRh-123) was introduced to ZnS: Cu, Co systems, and the persistent luminescence could still stimulate the TBrRh-123 for photodynamic therapy. In this way, the radiation dose applied can be reduced considerably and the PC3 human prostate tumor-cells can be damaged by the generated cytotoxic substances. Another X-ray activable polyethylene glycol (PEG) conjugated $SrAl_2O_4$: Eu^{2+} system was reported by Yang's group.[146] This nanocomposite can act as a good optical probe for repeatable high-sensitivity imaging for deep-cancer diagnosis. The broad emission band (450-700 nm range) of this scintillator was obtained from X-ray

illumination and the luminescence intensity raised gradually with the growth in X-ray tube voltage (as indicated in Figure 2e). With X-ray radiation, high-energy photons were absorbed by the host for the excitation of electrons and the excited electrons were then captured in trapping states. Subsequently, the trapped electrons were gradually released from the trap states and transmitted to the $4f^6 5d$ state of Eu^{2+} to radiate photons by the radiative transition (See Figure 2f-h). And this modified scintillator system demonstrated satisfactory optical stability under several X-ray illumination cycles (See Figure 2i). The medical imaging was conducted in human liver cancer-bearing mouse after injecting this scintillator into tumor. When re-excited by X-ray, the afterglow intensity in tumor-tissue was over 30 folds stronger than that detected at one-hour post injection, which indicated the great potential of X-ray/afterglow for dual model bio-imaging application.

In another dual-model imaging, X-ray serves as the single light source and the rare-earth ions doped core-shell-shell Nano-scintillator acts as the single contrast medium to attenuate and convert X-rays energy. As indicated in **Figure 3a**, hexagonal $NaGdF_4$ can serve as the host because Gd^{3+} was high-Z, high K-edge energy ions with a large X-ray mass attenuation coefficient and has the potential to activate other photosensitive Ln^{3+}.[147] Eu^{3+} acts as an emission center in the core, making the absorbed X-ray convert into light-emission in visible range possible. And the inner-shell Ce^{3+} delivers the absorbed X-ray energy to neighboring Gd^{3+} and then to the emission center of Eu^{3+}. $NaLuF_4$ builds the outermost shell to restrain surface quenching and further promote the X-ray attenuation ability originating from Lu^{3+}. The X-ray can generate electron-hole pairs when the radiation energy is equal to/greater than the host bandgap. The photosensitive rare-earth ions can be stimulated through the relaxation process including radiative transition, thermal dissipation, and energy transfer process. (See Figure 3b). The optimal proportion of the core-shell-shell structured nanocomposite is indicated in Figure 3c. In this material, the high-resolution three-dimension CT imaging can be obtained to accurately display the relative spatial position of bone structure and microstructure in the tumor-site (Figure 3d). But single CT imaging cannot provide function information on cancer in detail. The optical data from various angles can be obtained by camera and further remodeled to tomographic photographs, and the luminescent region and intensity vary in different slices. The feature and structure information of targeted cancer can be imaged comprehensively, which indicates that the dual-model strategy is a promising bio-imaging mode for pathological diagnosis.

5.3 Common Scintillating Materials for X-ray Imaging

Scintillators have been developed over a century[32], and they played a vital role in the detection of X-ray, γ-ray, α-particle, β-particle, and even for Higgs boson today.[148] Among these scintillating materials, CsI:Tl was one of the most commonly used conventional scintillating crystals discovered in the year 1951.[149] This scintillator has a relatively high LY (66,000 photons/MeV), a fast response time of 800 ns, and an emission band peaked at 550 nm which matches well the most sensitive range of the semiconductor based photodetector.[60] Additionally, it has a medium-density of $4.53 g/cm^3$ and a relatively high effective atomic number (Z_{eff}=54), and it also allows the manufacture of micro columnar films. Benefited from its low production cost, the CsI:Tl scintillator has been widely applied in the field of X- /γ-ray spectroscopy, homeland security, radiotherapy, and radiological imaging.[18] Nevertheless, the unwanted PL will induce the trouble of pulse pileup in high-count-rate scintillation application, impeding its utilization in high-speed imaging as well as computer

tomography.[19, 150] Although this material has shown superior performances for practical applications, it still suffers from the serious afterglow. Therefore, the approach for restraining PL in CsI:Tl based scintillating material has been sought actively over the past two decades.

Digital radiography technology converts X-ray images into electronic signals and shows on a digital displayer, which is an advanced X-ray imaging achievement that has been extensively used in clinical applications such as chest X-ray (CXR), C-arm X-ray system, mammography, and dental.[151] In a digital radiography system with indirect conversion, the scintillating material converts the incoming X-ray into visible-light emission, and then the emitted light can be converted into electric signals by the photodiode array. The visible-light emission in traditional scintillator scatters in all directions and hence degrades the spatial resolution. In the recent two decades, novel scintillating materials like pixelated Gd_2O_2S:Tb[152] (GOS) and CsI:Tl,[153-154] have already been developed to restrain the scattering of emitted light. The flexibility of scintillators is a key factor for further upgrading digital radiography systems. For X-ray imaging in dental diagnosis, applying flexible intraoral X-ray detectors weakens the discomfort aroused from the rigidity of traditional detectors for patients. Compared with CsI:Tl, the flexibility of GOS based scintillating matter is much improved since GOS is usually hybridized with organic materials. And the GOS based scintillator in dome-grooved structure obtains clearer X-ray images with improved spatial resolution.

5.4 Pb Based Scintillating Materials

5.4.1 Organic-inorganic Hybrid Perovskite-structured Pb-halide Scintillating Materials

Besides doped lanthanide scintillators, Pb-halide perovskites are another catalog of the heavy element based scintillating family emerging in the exploit of advanced ionizing radiation sensors due to the tunable emission wavelength, good charge carrier mobilities, direct charge clustering capability as well as good timing properties.[73, 155-156] These perovskite-like materials are a series of crystals in octahedral ABX_3 lattice, in which B is occupied by Pb, and X is occupied by halogen. A is occupied by a monovalent cation such as $CH_3NH_3^+$ (MA) or Cs^+ locating at the center of cubes constituted by eight PbX_6 groups. Bulk crystals, thin films and nanoparticles/QDs formed Pb-halide perovskites can be easily prepared by soft chemistry methods, so with no need for ultra-high vacuum technique, the preparation cost is rather reasonable. However, the existence of toxic Pb element has caused the environmental and health risks in the applications. Meanwhile, their low resistance to the humidity and temperature often leads to the degradation of performance and limits the application range.

Among Pb-halide perovskites, organic-inorganic hybrid Pb-halide perovskite-structured single crystals can serve as excellent scintillating materials due to their low manufacturing cost, high LY, short decay time in the nanosecond range, and low inherent trap density.[23] $MAPbX_3$ based scintillators yield markedly large absorption cross-section for X-rays owing to the high-Z atoms (Cl, Br, I and Pb).[131, 157] Hybrid $MAPbX_3$ perovskites have exhibited satisfactory scintillating performance for photo-electronic devices such as field-effect transistors,[158] luminous devices[159-160] and high-sensitivity detectors in the visible range.[161] As indicated in **Figure 4a**, $MAPbI_3$ and $MAPbBr_3$ crystals have the classical 3D perovskite structure, with $CH_3NH_3^+$ occupying the interstitial sites.[162-163] By contrast, EDBE-$PbCl_4$ pertains

to $APbX_4$ (A denotes bidentate organic cation) 2D perovskite crystal family.[164] By UV excitation, green and white colors are emitted from $MAPbBr_3$ and EDBE-$PbCl_4$ respectively, while we cannot observe the shining of $MAPbI_3$ because it emits in the NIR range. Based on the emission wavelength in Figure 4b, $MAPbBr_3$ (centered around 560 and 550 nm) and EDBE-$PbCl_4$ (centered at 520 nm) appear to be the potential candidates for the scintillators coupled with an avalanche photodiode (APD).[16] In order to match the optimum sensitivity range of high quantum efficiency APD, the emission spectrums can be further modulated through the substitution of cations/halides in the lattice. Low-temperature scintillation under X-ray excitation under 60 keV X-ray excitation (Figure 4c-d) have indicated that the LY can achieve as high as 120000 photons/MeV in EDBE-$PbCl_4$ at the temperature of 130 K, and even above 150000 photons/MeV in $MAPbI_3$ and $MAPbBr_3$ at 10 K. Thermoluminescence (TL) data illustrate that perovskite-structured scintillators have relatively lower trap density than classical oxide scintillating crystals.[165-166] The luminescence yield of these two 3D perovskites decreases remarkably at room temperature, while the corresponding LY of this 2D perovskite is less influenced by thermal quenching owing to the large exciton binding energy. Thus, the scintillating performances can be further improved by perovskite structure modulation and dimensionality reduction.

Another successful case of organic-inorganic hybrid perovskite Pb-halide scintillators is layered $(C_6H_5C_2H_4NH_3)_2PbBr_4$. According to the emission spectra indicated in Figure 4e, A sharp scintillating peak can be discovered at 437 nm ascribed to the exciton emission from the inorganic layer. The bulk $(C_6H_5C_2H_4NH_3)_2PbBr_4$ sample exhibits excellent scintillating performance with a fast response time of 11 ns (Figure 4h) and an extremely high scintillation LY(under synchrotron X-ray irradiation of 67.4 keV) of 14000 photons/MeV (Figure 4f-g), 1.4 times higher than that of conventional inorganic scintillator GSO: Ce (10000 photons/MeV).[83] Figure 4i indicates that the PL levels of $(C_6H_5C_2H_4NH_3)_2PbBr_4$ and GSO: Ce were 5 and 15 ppm respectively, and the afterglow effect of this hybrid organic-inorganic perovskite is nearly equivalent to those of common inorganic scintillating materials $CdWO_4$ and BGO.[167] Figure 4j suggests that the pulse height channel (scintillating LY) is proportional to the incident radiation energy, which means $(C_6H_5C_2H_4NH_3)_2PbBr_4$ is a potential scintillating material for the detection of γ-rays in 122-662 keV range. These experimental data suggest that hybrid organic-inorganic layered Pb-halide perovskites are promising scintillator for X-ray/γ-ray detection. Given the potential of hybrid Pb-halide perovskites, further attempts should be made to fabricate novel materials for γ-ray and X-ray scintillation. The scintillation LY of perovskite crystals are expected to be further enhanced through the addition of rare earth dopants such as Ce^{3+} [61, 168], or by the mixture of halides to modify the bandgap.[15] And the optimum operating temperature can be increased by the design of wide bandgap layered hybrid organic-inorganic perovskite crystals with minimal quenching effects.[83]

5.4.2 All-inorganic Pb-halide Perovskite-structured Nanoscintillators

A wide variety of all-inorganic scintillators containing heavy metal atoms such as Pb have been analyzed in-depth for X-ray excited scintillation. Most of these scintillators are in bulk-form prepared by the Czochralski approach, and ambient temperature above 1,700 °C is required.[32] For bulk crystals like $PbWO_4$, a rational distance for exciton transition is typically required to migrate electrons/holes for following trapping process at recombination centers. Nevertheless, excessive exciton migration is disadvantageous as it generates afterglow emission and restrains the efficiency of scintillation. And

typical rare-earth activated scintillating materials like Tl doped CsI and Ce doped $YAlO_3$ can not generate multicolor scintillation owing to their fixed transition energy gap.[169-170] The emission spectrums of typical bulk scintillators such as $PbWO_4$, BGO, Tl activated CsI and Ce activated $YAlO_3$ are almost unchanged and demonstrates a broad peak with a wide full width at half maximum. This inherent insufficiency limits the tunable multicolor emission for visualized medical imaging under high-energy X-ray excitation.

However, the novel scintillating nanocrystal is developed based on charge carrier migration mechanisms in typical scintillators. For conventional bulk scintillators, incident kiloelectronvolt scale X-rays motivate Pb atoms to generate numerous hot electrons by the photoelectric effect. These excited electrons are quickly thermalized to form low-energy excitons, which can subsequently be migrated to defect states or dopant states for radioluminescence. This indicates that high-energy X-ray in the KeV range can be converted into a large number of low-energy emissions in visible light range through direct bandgap transition in Pb-halide perovskites. With enormous attempts, novel scintillators that are highly X-ray sensitive, solution-processable, and integrable to flexible substrates at lower synthesizing temperatures have been reported in recent years. The perovskite-structured $CsPbX_3$ nanocrystals are prepared by modulating the interaction of Cs oleate with a series of PbX_2 precursors through the hot-injection-solution approach.[171] By this synthetic method, $CsPbBr_3$ nanoparticles have been synthesized successfully and exhibit unique X-ray photosensitivity for X-ray optical imaging.

Under X-ray beam irradiation, the perovskite-like $CsPbBr_3$ nanoparticles yield narrow and tunable multicolor emissions, which makes it possible for the high-efficiency X-ray visualized imaging.[7] Combined with the different X-ray stopping ability of metal and insect tissue, the metallic needle inside the insect body can be clearly displayed by phase-contrast imaging detected by a standard digital camera (**Figure 5a-c**). As indicated in Figure 4d, the detection limit for X-ray is calculated to be only 13 nGy s^{-1}, which is over 400 times lower than the dose rate generally applied for X-ray based medical radiography.[131] This nanoscintillator also has a good photostability and a very fast time response of 44.6 ns, which is a crucial scintillating property for X-ray bio-imaging (Figure 5e, f). The $CsPbBr_3$ nanoscintillator based commercial flat panel X-ray detector (Figure 5g) is applied to image the internal structures of an iPhone under a relatively low X-ray dose (Figure 5h). And this $CsPbBr_3$ nanoscintillator based X-ray flat panel detector has a relatively high modulation transfer function value at a certain spatial resolution (Figure 5i). Therefore, this novel perovskite-like nanoscintillator is very promising in low X-ray does radiographic diagnosis.

5.5 Lead-Free Halides as Sensitive Scintillators

Pb halide perovskite-like scintillators have recently attracted extensive research interests due to their material features on low detection limits, adjustable emitting wavelengths, easy assembly, and manufacturing. As described above, heavy-metal Pb based scintillating materials are widely applied for many X-ray detection fields, especially in medical imaging. However, compared to traditional scintillators such as CsI-Tl[172], LYSO[172], and GOS[173], the Pb-halide perovskites exhibit relatively lower LY under X-ray radiation[73] and the toxicity of the soluble-Pb in these perovskites severely limit their applications in the biomedical domain. Therefore, the

attempts to develop novel lead-free scintillators are of great significance in terms of reducing cytotoxicity and avoiding environmental pollution.[174]

Rb_2CuBr_3 is a recently reported lead-free scintillator in a one-dimensional (1D) crystalline structure with strong carrier confinement and singularly high photoluminescence quantum yield (PLQY) of 98.6% in the violet emission region. And the strong X-ray absorption ability with negligible self-absorption from the emission of self-trapped excitons (STEs) results in an extremely high LY of over 91000 photons/MeV (under 30 keV X-ray excitation).[174] **Figure 6a** illustrates the crystalline structure of Rb_2CuBr_3, in which a Cu atom is surrounded by four Br atoms, constituting a distorted tetrahedron $[CuBr_4]^{3-}$. Similar to previous low-dimensional metal halide perovskite-like materials with STEs,[175-176] a large Stokes shift is presented in Figure 6b. The negligible photoluminescence and photoluminescence excitation (PLE) overlapping indicates a weak self-absorption effect, which is a prior-condition for achieving high LY. The relatively long decay time of 41.4 μs (Figure 6c) suggests that the application prospects of Rb_2CuBr_3 in ultrafast scintillation applications such as nuclear reaction monitoring and medical imaging are affected. The near-unity PLQY of Rb_2CuBr_3 calculated in Figure 6d is comparable with Pb-halide perovskites[177-178] and superior to previous lead-free inorganic perovskites[179-180]. Because of its 1D electronic dimensionality, a relatively large activation-energy is observed (Figure 6e). We can see in Figure 6f that the absorption coefficient of Rb_2CuBr_3 is much higher than CsI: Tl and a little lower than LYSO in the photo-energy range for medical digital radiography (0.018-0.030 MeV). As indicated in Figure 6g, the Rb_2CuBr_3 is assembled onto the silicon photomultiplier (SiPM), a sensitive photodetector for detecting photo-signals even in single-photon level and it has been widely applied in dynamic X-ray imaging. And the emission band of Rb_2CuBr_3 is situated very close to the maximum photodetection efficiency region of SiPM. As indicated in Figure 6h, the detection limit (121.5 nGy_{air}/s) of Rb_2CuBr_3 based photodetector is much lower than the requirement for X-ray diagnostics (5.5 $\mu Gy_{air}/s$),[131] which further enables its applications in low-dose X-ray imaging. The LY of Rb_2CuBr_3 is higher than some commercial scintillating materials including GOS and CsI:Tl, which significantly surpass previously reported $CsPbBr_3$ nano-scintillator. The only flaw of this material is due to the intrinsic radioactivity for the presence of radioactive isotope ^{87}Rb, which often results in a constant background signal and affects the detection of low-dose X-ray or Gamma rays. Therefore, the perovskite-like Rb_2CuBr_3 scintillator not only has satisfactory scintillating performance for low-dose X-ray radiography but also avoids the severe trouble caused by high toxicity of Tl and Pb ions. Integrating this nontoxic metal-halide scintillator with matched photodetector panels is of great potential for the applications in dynamic X-ray imaging.

5.6 Scintillating Metal-Organic Frameworks

In order to improve the image quality and weaken the radiation exposure on patients, the new generation X-ray imaging techniques like single-photon computed tomography (SPCT), CT, and PET are very demanding for highly sensitive scintillating materials.[43] Conventional X-ray to visible-light converters is mainly formed by heavy atoms/lanthanides based scintillators such as Pb-halide/lead-free perovskites,[7, 174] BGO,[181] LSO: Ce and LYSO: Ce,[95] $LaBr_3$: Ce^{3+} and SrI_2: Eu^{2+} [92-93]. However, it is still challenging in exploring novel scintillators to enable the medical detections under lower X-ray radiation dose with faster evaluation.[182] Organic nanocrystals like stilbene, naphthalene as well as anthracene exhibiting high

attenuation-constant can serve as good scintillating materials for β-ray or hot-neutron but exhibit unsatisfactory efficiency on X-ray detections.[183-184] Metal-organic frameworks (MOFs) are a new class of scintillators composed of metal-atoms or metal-clusters connected with nodes and organic bridging ligands.[185] With defined porous structures, MOFs exhibit excellent energy conversion efficiency to X-rays and provide a structurally tunable platform for different application scenarios.[186] The functional motifs of organic emitters enable them to respond faster to X-rays than traditional commercial inorganic scintillators.[187]

For instance, the integration of high-Z and high oxidation state in UVI materials results in high attenuation efficiency toward X-rays and strong green light emission generated by the charge-transfer from ligand to metal. This suggests that the UVI materials are expected to serve as efficient scintillating candidates for X-ray detection and the observable light emission in a uranyl-organic framework (SCU-9) are very promising features for practical applications in medical imaging fields. SCU-9 also exhibits the superiority of significantly reducing the non-radiative relaxation in the process of excitation, which further improves the conversion efficiency. The emission intensity shows an essentially linear correlation with the exposed X-ray dose, and this parameter is comparable to that of the commercial scintillator CsI: Tl. In addition, SCU-9 also exhibits decreased hydroscopicity, enhanced X-ray radiation resistance, and reduced efficiency.[188]

6. X-ray Induced Scintillators for Photodynamic Therapy

At present, various X-ray activatable scintillators have attracted increasing research interests, especially for clinical therapy. This is mainly because modern X-rays based imaging instruments became increasingly sophisticated to improve the image resolution for clinical diagnosis and pathology researches. For clinical purposes, it is crucial to realize that specific tumor targets are treated in various energy ranges. Low energy irradiation is in the 40-100 kV range. These superficial X-rays (kV-range beams) are therapeutic only for skin tumors because they cannot penetrate the tissues deeper than 5 mm. Sub-surface cancer demands supervoltage X-ray beams in medium energy region (200 kV-1 MV). And deep X-rays in the megavoltage range are currently utilized to heal the cancers deeper than 2 cm, with high-energy irradiation within 4-25 MV.[90]

Realizing effective therapy for deep-seated cancer is a major challenge for modern photodynamic therapy (PDT) owing to the impediments on delivering radiation energy into the deep tissue/organ. Due to the great tissue-penetration of X-ray, it exhibits the capacity to serve as the excitation light source to activate photosensitizers (PSs) that accumulate in sub-tumors. Whereas traditional PSs cannot absorb high-energy X-rays for the production of $^1O_2$ directly. To improve the limited tissue-penetration in conventional PDT, the integration of X-ray induced PDT and radiation therapy is proposed to promote the therapeutic efficacy for deep tumors. Recently, various nanoparticles (NPs) are tested to be potential candidates for this combination. They not only act as carriers for loading various PSs but also serve as energy transducers to boost the photo-activation process by converting the absorbed X-ray radiation energy to loaded PSs.[189-190]

6.1 The Mechanism of X-ray Induced Scintillating Materials for Photodynamic Therapy

The mechanism of X-ray stimulated NPs for PDT is mainly involved in the production of $^1O_2$, as indicated in **Scheme 2**. After the nano-photosensitizers have been loaded at the tumor tissue, X-ray irradiation will be utilized to activate the encapsulated metal to produce light emission.[191] The emission light can then be absorbed to motivate the nearby PSs for X-ray activated PDT. Wide bandgap materials are adopted for the conversion of X-rays to photon radiation in the UV/visible range. This transformation process happens within 1 picosecond. A cascade interaction between X-ray photons and the lattice of scintillating nanoparticles (ScNPs) proceeds via Compton scattering and photoelectric effects. During this process, numerous hole-electron pairs are generated and thermalized in CB and VB respectively. Then these charge carriers eventually generate excitons and transfer through the material. Repeated electrons trapping at defect sites may also take place and the energy loss is mainly caused by the nonradiative transition. The recapture of electrons/holes within the bandgap can give rise to considerable delay for the migration of charge carriers. This recapturing stage is unpredictable since native point defects, flaws, surfaces and interfaces can create additional energy states in the bandgap, which may bring about strong modification or degradation rather than satisfactory intrinsic scintillating performance. At the last stage, radio-luminescence is generated by continuous trapping of electrons/holes at the emission center and the subsequent radiative recombination.[1, 192] In the meantime, the ET process from ScNPs will stimulate the nearby PSs jumping to S_1 stage, and this will lead to the generation of $^1O_2$ (very toxic to cells) during the electrons transmitting back to S_0.[90]

The typical X-ray induced PDT can be divided into three main processes: (1) the Nano scintillating materials are excited by X-rays to produce X-ray excited optical luminescence. (2) Subsequently, the generated X-ray excited optical luminescence is absorbed by adjacent, well-matched photosensitizers to manufacture cytotoxic singlet oxygen ($^1O_2$) which can directly destroy the cell-membrane phospholipid of cancer cells, and meanwhile, the absorbed X-ray radiation can produce radical species and damage the DNA duplex. (3) The generated ROS causes the destruction of the tumor by the combination of radiotherapy and PDT processes to realize effective cancer therapy. Thus, based on the efficient ET process in the photosensitizer loaded scintillating nano-materials (nano-sensitizers), X-ray radiation can be utilized as the excitation light source to induce deep-tumor PDT. However, the excitation energy of the X-ray radiation applied in clinical radiotherapy ranges from hundreds of keV to MeV. Consequently, most conventional photosensitizers applied for deep-tumor PDT can hardly be activated by X-ray radiation energy in the clinical range efficiently. In this case, a physical transducer is needed to absorb the X-ray radiation energy and further transfer it to photosensitizers to generate cytotoxic $^1O_2$ for the killing of cancer cells.[193]

6.2 Applications of Scintillating Materials in Photodynamic Therapy

The Ce^{3+} doped $NaCeF_4$: Gd, Tb ScNPs has been reported as a successful case for X-ray induced PDT application. This ScNPs are synthesized in the homogeneous rod-like form for X-ray activated radio dynamic therapy (**Figure 7a**). Owing to the sensitization effect of Ce^{3+}, Tb^{3+} can generate luminescence with X-ray radiation. Ce^{3+} and Tb^{3+} absorb the energy from secondary electrons produced by X-ray to generate $\bullet O^{2-}$ for radio dynamic therapy. With the native absorption of X-ray radiation via rare-earth ions, this doped ScNPs based scintillating system can simultaneously serve as the contrast medium for CT imaging and X-ray absorber for radiotherapy (Figure 7b). The

production of $\bullet O^{2-}$ and •OH with $NaCeF_4$: Gd, Tb ScNPs-PEG under X-ray radiation (Figure 7c, d) exhibits the capacity for serving as the X-ray sensitizer to promote radiotherapy (Figure 7e, f). The ScNPs-PEG has low cytotoxicity, as indicated in Figure 7g. The ScNPs-PEG modulated radiotherapy could efficiently boost the lethality for cancer-cell by increasing the local X-ray dose (See Figure 7h, i). The light emission intensity is remarkably enhanced when cells synchronously treated by the ScNPs-PEG and X-ray illumination, which indicates that much more $\bullet O^{2-}$ has been generated in X-ray induced PDT (Figure 7j). The therapeutic mechanism of ScNPs-PEG for synchronous tumor radiotherapy and PDT were established on the enhancement of DNA damage (Figure 6k) and $\bullet O^{2-}$ production.

However, it is still a challenge that traditional radiation therapy combats tumor by applying high-doses radiation to kill cancer cells, which is also destructive to normal cells owing to the nonspecific-targeted radiation. The combination of traditional radiation therapy with PDT exhibits the potential capacity to achieve better therapeutic efficacy and reducing the harm to normal cells under lower radiation doses. This low radiation dose X-ray activated NPs based therapy was first reported by Chen's group in the year 2006.[194] They applied ScNPs to deliver porphyrins (as PSs) to the tumor site in vivo. The NPs transfer the absorbed X-ray energy to the PSs, which results in the generation of $^1O_2$ to kill cancer cells.

7. Summary and Outlook

7.1 New Mechanism for X-ray Scintillating Materials

It is a fact that crystal defects are inevitable in the synthesis process. Although X-ray scintillation has been studied a lot, the underlying mechanism and the roles that the defects play is still under discussion. Generally, defects can be classified into three types (point, linear as well as three-dimensional defects) based on their shape and size and each defect category has the potential to affect the scintillating properties. Since the positions of electronic centers locate very close to the bottom of the conduction band (CB), it is possible to differentiate the impacts caused by different defect types on scintillating performance. Despite a fast exchange of electrons between the shallow polaron and RE distorted regular centers with CB which contribute to the scintillation, there is also a flow of electrons moving toward the deep traps. For instance, at high WO_4^{2-}-RE centers, this outflow becomes very crucial because it gives rise to an obvious decrease in LY. Thus, the strong demand for radiation hardness of the lead tungstate crystal imposes the doping with trivalent RE-ions which results in the decrease of crystal LY. Therefore, the possibility of satisfying both high LY and good radiation hardness is to improve the quality of crystal structure based on the existing synthetic technology. [195]

Native point defects always exist in a certain concentration in a crystal under thermodynamic equilibrium. This kind of defects induce the capture of charge carriers and initiate the energy storage process, and in some crystals, the internal point defects have absorption especially in the UV region, which is very likely to reduce the material transparency at certain emission bands. Anion Frenkel (a-Fr) defect is a typical intrinsic defect, which consists of a neutral vacancy-interstitial pair. This is formed when an anion is displaced off the original lattice site into an interstitial site, which has been identified as the dominant defects in many fluorides and oxides[196-199]. The a-Fr defect has shown a significant effect on other properties such as ion conduction or thermal conductivity[197, 199-200]. Until now, such defect and its correlation with the

luminescence properties have rarely been discussed in $NaREF_4$ materials before. For $NaREF_4$, the a-Fr is constructed by the F vacancy (V_F) and interstitial F (I_F). Previous works have utilized the XRD characterization to identify the slight lattice change induced by the evident ratio change of V_F[201]. However, whether these V_F are a simply intrinsic vacancy or belong to the vacancy-interstitial pair of a-Fr are still challenging to determine. The vacancy formation usually occurs during the synthesis while the a-Fr defects are formed by the thermal perturbation or luminescence excitation.

Therefore, we propose a new a-Fr dominated mechanism for the PL performance in $NaREF_4$ (**Scheme 3**). Although this mechanism is also based on the intrinsic defects in the materials, it proposed a completely different concept of defect-assisted PL as our previous works. The previous works have carefully demonstrated the surface defect states induced level-matching induced surface resonant quantum tunneling (LM-SRQT) effect to prolong the emission time. In comparison, our new mechanism is proposed based on the relaxation of charged a-Fr excited by the X-ray. Distinct with the conventional concept of a-Fr in the previous defect investigation, we propose that the displacement of F atom to form the a-Fr is accompanied by the electron due to the appropriate excitation by high energy X-ray. Within this situation, a novel intrinsic defect type as the charged a-Fr is formed within the lattice. This novel type of charged a-Fr possesses the charged V_F sites that play as the optimal trap for electrons as well as transferring the electrons to the nearby Tb sites. During the relaxation of the formed transient a-Fr, two different electron transfer pathways have been illustrated. For the close distance a-Fr, the recovery of the F anion indicates the electrons also relax back from the trap states to VB. Meanwhile, for the large distance a-Fr in the lattice, the interstitial F anions with electrons substitute the position of nearby F atoms, which not only transfers the electrons but also shows no energy loss. This substation process further extends the relaxation time of the activated electrons within a-Fr. Moreover, the formation of such a novel charged a-Fr also induces the appropriate trapping levels for electrons, which determines the relaxation time of electrons in the V_F states and further influences the PL performance. The long relaxation time of the charged a-Fr in the lattice is the essential factor for the superior PL of Tb-doped $NaREF_4$. The introduction of Tb activates the energy transfer paths with stronger PL performance. For energy levels near Tb, the electron can transfer towards Tb levels through the tunneling. For those electrons at the lower level, the electrons can experience the electron collision from CB, in which the energy is sufficient to support the electron towards higher Tb levels. To further prove our proposed mechanism, we systematically summarize both neutral and charged a-Fr regarding the V_F states.

7.2 Challenges for X-ray Scintillation Technique

The high-energy X-ray technique is a promising tool for killing deep-seated cancer cells owing to its amazing penetration ability in vivo and ionizing radiation nature that results in apoptosis. Scintillators are excellent energy transducers that can absorb and convert X-rays into visible light, serving as potential contrast agents for medical radiography. We have elaborated on the progress in scintillators from early heavy metal ions based compounds ($CaWO_4$, NaI: Tl^+, and $Bi_4Ge_3O_{12}$) to the latest perovskite-like scintillating materials[7], especially in the perspective of clinic diagnose/therapy. The scintillating performance can be tuned by choosing appropriate host lattice, tailoring morphology and structure/size, changing dopant types and concentrations, and enhancing the ET process. Rapid development in nanotechnology and materials science engineering also accelerates the exploitation of various X-ray sensitized scintillating materials that

synergize radiotherapy and other therapeutic modalities, realizing optimal energy accumulation to ionizing radiation at a relatively lower dose.[202] Newly designed scintillating nanocrystals with high light yield and tunable luminous properties have already played significant roles in radiation-induced *in-vivo* biochemical reactions.

Whereas, there are still some challenges in the design and exploitation of novel high-energy radiation sensitized scintillating systems for medical purposes. Owing to the visible light emission, the endogenous molecules like water, hemoglobin, carbohydrates, and fats will cause considerable scattering and absorbance, which gives rise to severe signal decay in proportion to bio-imaging depth.[203] Compared to visible light, emissions in the near-infrared (NIR) range exhibit better penetrability, especially in skin and blood.[204] Therefore, exploring novel scintillators emitting in the NIR range is of great potential to improve the resolution and sensitivity for deep-tissue in vivo imaging. Besides the dopant-tuned strategy,[17, 205-206] the abundant defect states in the host bandgap should also be treated as promising candidates for manipulating the scintillating performance.[207] The electronic and optical properties of defect states simulated under density functional theory can also offer a good reference to guide the development of novel defect-tuned scintillators for deep-tissue NIR imaging. As for biomedical researches, more attention should be paid to biological activity and biocompatibility. Rational decoration of functional group for specific recognition and satisfactory circulation/retention time of the scintillating systems are both demanded to facilitate the effective accumulation at the target tumor-site. Ideal nano-scintillators should target the specific hypoxic tumor-site and be harmless to healthy tissues/cells, which can be achieved by external irritation and/or specific biochemical responses to the microenvironment of cancer-cell. The in vivo optical performance of scintillators is usually affected by their morphology, structure, size, chemical constitution, and surface modification effects. Thus, further investigations and characterizations on existing scintillating materials in various states also have bright prospects. Finally, for medical radiography and clinic therapy, the intratumor injected scintillators are highly desired to be low cytotoxic or biodegradable, easily excreted, or cleared.

7.3 Future Research Trends

Based on the present research achievements and progress, we have proposed the potential research trends for the X-ray activated scintillators. First of all, the theoretical calculations should be introduced to investigate the precise band structures and the mechanisms of charge and energy transfer. Our previous works have confirmed that the significant role of theoretical calculations in understanding the in-depth mechanisms to improve the PL performances as well as broadening the applications. Then, further material engineerings such as co-doping, nanostructure modulations on the conventional scintillating materials is still of significance to further enhance their performances. Meanwhile, the rare-earth halides are promising candidates due to a very high light yield and unprecedented energy resolution in the domain of energy-relevant for medical imaging applications. The rare-earth doping strategy is also an effective approach to improve the performances of oxides in PET scanners.

In conclusion, materials engineering and nanoscience have offered excellent technical supports for the developments of X-ray activated scintillators in medical radiography and deep-tumor therapy. Novel nanoscale scintillating materials are very prospect to serves as a contrast medium in low dose CT imaging. Additionally, due to the nearly

unlimited penetration depth of X-ray, the corresponding scintillator exhibits great potential for the targeted therapy of deep-seated tumors. Due to their sufficient X-ray attenuation coefficient, it will reduce the damage to healthy tissues and organs in radiotherapy. Exploring advanced X-ray activated nanoscintillator will remain a frontier research topic for the progress of radiographic and therapeutic facilities for the diagnosis and treatment of deep-tumor. In future clinical trials, close co-operation between scientists, engineers, physicians, and pharmacists is urgently demanded in the accurate evaluation of the treatment efficacy and side effects of the intra-tumor injected scintillators, which is very crucial for further improving the cure rate of cancer and markedly prolonging the life of the patients.

Acknowledgements
The authors gratefully acknowledge the support of the Natural Science Foundation of China (Grant No.: NSFC 21771156), and the Early Career Scheme (ECS) fund (Grant No.: PolyU 253026/16P) from the Research Grant Council (RGC) in Hong Kong.

References

[1] G. Blasse, Scintillator Materials. *Chem. Mater.* **1994,** *6*, 1465-1475.
[2] H. Wei; J. Huang, Halide Lead Perovskites for Ionizing Radiation Detection. *Nat Commun* **2019,** *10* (1), 1066-1077.
[3] P.-Y. Guo; C. Sun; N.-N. Zhang; L.-Z. Cai; M.-S. Wang; G.-C. Guo, An Inorganic–Organic Hybrid Photochromic Material with Fast Response to Hard and Soft X-Rays at Room Temperature. *Chemical Communications* **2018,** *54* (36), 4525-4528.
[4] Y. Cui; J. Zhang; H. He; G. Qian, Photonic Functional Metal–Organic Frameworks. *Chemical Society Reviews* **2018,** *47* (15), 5740-5785.
[5] H. N. Chapman; P. Fromme; A. Barty; T. A. White; R. A. Kirian; et al., Femtosecond X-Ray Protein Nanocrystallography. *Nature* **2011,** *470* (7332), p.73-77.
[6] X. Duan; J. Cheng; L. Zhang; Y. Xing; Z. Chen; Z. Zhao, X-Ray Cargo Container Inspection System with Few-View Projection Imaging. *Nuclear Inst & Methods in Physics Research A* **2009,** *598* (2), 439-444.
[7] Q. Chen; J. Wu; X. Ou; B. Huang; J. Almutlaq; A. A. Zhumekenov; X. Guan; S. Han; L. Liang; Z. Yi; J. Li; X. Xie; Y. Wang; Y. Li; D. Fan; D. B. L. Teh; A. H. All; O. F. Mohammed; O. M. Bakr; T. Wu; M. Bettinelli; H. Yang; W. Huang; X. Liu, All-Inorganic Perovskite Nanocrystal Scintillators. *Nature* **2018,** *561* (7721), 88-93.
[8] S. Sahi; S. Magill; L. Ma; J. Xie; W. Chen; B. Jones; D. Nygren, Wavelength-Shifting Properties of Luminescence Nanoparticles for High Energy Particle Detection and Specific Physics Process Observation. *Scientific Reports* **2018,** *8* (1).
[9] M. Nikl, *Nanocomposite, Ceramic, and Thin Film Scintillators*. Pan Stanford Publishing Pte. Ltd.: Singapore, 2016; p 1-24.
[10] Y. Wang; X. Yin; J. Chen; Y. Wang; Z. Chai; S. Wang, Gleaming Uranium: An Emerging Emitter for Building X-Ray Scintillators. *Chem. Eur. J.* **2020,** *26* (9), 1900-1905.
[11] Y. Zorenko; V. Gorbenko; T. Zorenko; P. Malinowski; V. Jary; R. Kucerkova; A. Beitlerova; J. A. Mares; M. Nikl; A. Fedorov, Luminescent and Scintillation Properties of Bi^{3+} Doped Y_2sio_5 and Lu_2sio_5 Single Crystalline Films. *Journal of Luminescence* **2014,** *154*, 525-530.
[12] Y. Zorenko; V. Gorbenko; T. Zorenko; V. Savchyn; A. Voloshinovskii In *Luminescent and Scintillation Properties of $Cawo_4$ and $Cawo_4$:Bi Single Crystalline Films*, International Conference on Oxide Materials for Electronic Engineering -

fabrication, properties and applications (OMEE-2014), 26-30 May 2014; 2014; pp 253-254.
[13] K. Kamada; Y. Shoji; V. V. Kochurikhin; M. Yoshino; S. Okumura; S. Yamamoto; J. Y. Yeom; S. Kurosawa; Y. Yokota; Y. Ohashi; M. Nikl; M. Yoshino; A. Yoshikawa, 2 Inch Size Czochralski Growth and Scintillation Properties of Li^+ Co-Doped Ce:$Gd_3ga_3al_2o_{12}$. *Optical Materials* **2017,** *65*, 52-55.
[14] A. Yoshikawa; K. Kamada; S. Kurosawa; Y. Shoji; Y. Yokota; V. I. Chani; M. Nikl, Crystal Growth and Scintillation Properties of Multi-Component Oxide Single Crystals: Ce:Ggag and Ce:La-Gps. *Journal of Luminescence* **2016,** *169*, 387-393.
[15] M. D. Birowosuto; P. Dorenbos; K. W. Krämer; H. U. Güdel, Ce^{3+} Activated $Labr^{3-}Xix$: High-Light-Yield and Fast-Response Mixed Halide Scintillators. *Journal of Applied Physics* **2008,** *103* (10), 103517.
[16] M. D. Birowosuto; P. Dorenbos; C. W. E. van Eijk; K. W. Krämer; H. U. Güdel, High-Light-Output Scintillator for Photodiode Readout: $Lui_3:Ce^{3+}$. *Journal of Applied Physics* **2006,** *99* (12), 123520.
[17] Y. Wu; Q. Li; B. C. Chakoumakos; M. Zhuravleva; A. C. Lindsey; J. A. Johnson; L. Stand; M. Koschan; C. L. Melcher, Quaternary Iodide $K(Ca,Sr)I_3:Eu^{2+}$ Single-Crystal Scintillators for Radiation Detection: Crystal Structure, Electronic Structure, and Optical and Scintillation Properties. *Advanced Optical Materials* **2016,** *4* (10), 1518-1532.
[18] B. K. Cha; J. Hyung Bae; C.-h. Lee; S. Chang; G. Cho, The Sensitivity and Spatial Resolution Dependence on the Microstructures of Csi:Tl Scintillation Layer for X-Ray Imaging Detectors. *Nuclear Instruments and Methods in Physics Research Section A: Accelerators, Spectrometers, Detectors and Associated Equipment* **2011,** *633*, S297-S299.
[19] S. C. Thacker; B. Singh; V. Gaysinskiy; E. E. Ovechkina; S. R. Miller; C. Brecher; V. V. Nagarkar, Low-Afterglow Csi:Tl Microcolumnar Films for Small Animal High-Speed Microct. *Nuclear Instruments and Methods in Physics Research, Section A: Accelerators, Spectrometers, Detectors and Associated Equipment* **2009,** *604* (1-2), 89-92.
[20] M. Kobayashi; M. Ishii; K. Harada; I. Yamaga, Bismuth Silicate $Bi_4si_3o_{12}$, a Faster Scintillator Than Bismuth Germanate $Bi_4ge_3o_{12}$. *Nuclear Instruments and Methods in Physics Research Section A: Accelerators, Spectrometers, Detectors and Associated Equipment* **1996,** *372* (1), 45-50.
[21] W. Drozdowski; A. J. Wojtowicz; S. M. Kaczmarek; M. Berkowski, Scintillation Yield of $Bi_4ge_3o_{12}$ (Bgo) Pixel Crystals. *Physica B: Condensed Matter* **2010,** *405* (6), 1647-1651.
[22] G. C. Santana; A. C. S. de Mello; M. E. G. Valerio; Z. S. Macedo, Scintillating Properties of Pure and Doped Bgo Ceramics. *Journal of Materials Science* **2007,** *42* (7), 2231-2235.
[23] M. D. Birowosuto; D. Cortecchia; W. Drozdowski; K. Brylew; W. Lachmanski; A. Bruno; C. Soci, X-Ray Scintillation in Lead Halide Perovskite Crystals. *Sci Rep* **2016,** *6*, 37254.
[24] P. Kaur; D. Singh; T. Singh, Sm^{3+} and Gd^{3+} Co-Doped Lead Phosphate Glasses for Γ-Rays Shielding and Sensing. *Journal of Luminescence* **2019,** *209*, 74-88.
[25] H. Wang; B. Lv; Z. Tang; M. Zhang; W. Ge; Y. Liu; X. He; K. Zhao; X. Zheng; M. He; W. Bu, Scintillator-Based Nanohybrids with Sacrificial Electron Prodrug for Enhanced X-Ray-Induced Photodynamic Therapy. *Nano Letters* **2018,** *18* (9), 5768-5774.

[26] T. J. Hajagos; C. Liu; N. J. Cherepy; Q. Pei, High-Z Sensitized Plastic Scintillators: A Review. *Advanced Materials* **2018,** *30* (27), 1706956.
[27] D. G. Chica; Y. He; K. M. McCall; D. Y. Chung; R. O. Pak; G. Trimarchi; Z. Liu; P. M. De Lurgio; B. W. Wessels; M. G. Kanatzidis, Direct Thermal Neutron Detection by the 2d Semiconductor 6liinp2se6. *Nature* **2020,** *577* (7790), 346-349.
[28] G. H. V. Bertrand; M. Hamel; F. Sguerra, Current Status on Plastic Scintillators Modifications. *Chem. Eur. J.* **2014,** *20* (48), 15660-15685.
[29] C. Dujardin; E. Auffray; E. Bourret-Courchesne; P. Dorenbos; P. Lecoq; M. Nikl; A. N. Vasil'ev; A. Yoshikawa; R. Y. Zhu, Needs, Trends, and Advances in Inorganic Scintillators. *IEEE Transactions on Nuclear Science* **2018,** *65* (8), 1977-1997.
[30] L. H. Brixner, New X-Ray Phosphors. *Materials Chemistry & Physics* **1987,** *16* (3-4), 253-281.
[31] R. Hofstadter, Alkali Halide Scintillation Counters. *Physical Review* **1948,** *74* (1), 100-101.
[32] M. J. Weber, Inorganic Scintillators: Today and Tomorrow. *Journal of Luminescence* **2002,** *100* (1), 35-45.
[33] D. A. Pawlak; K. Kolodziejak; S. Turczynski; J. Kisielewski; K. Rożniatowski; R. Diduszko; M. Kaczkan; M. Malinowski, Self-Organized, Rodlike, Micrometer-Scale Microstructure of $Tb_3sc_2al_3o_{12}$−$Tbsco_3$:Pr Eutectic. *Chemistry of Materials* **2006,** *18* (9), 2450-2457.
[34] S. Liu; J. A. Mares; X. Feng; A. Vedda; M. Fasoli; Y. Shi; H. Kou; A. Beitlerova; L. Wu; C. D'Ambrosio; Y. Pan; M. Nikl, Towards Bright and Fast $Lu_3al_5o_{12}$: Ce, Mg Optical Ceramics Scintillators. *Advanced Optical Materials* **2016,** *4* (5), 731-739.
[35] J. Li; X. Du; G. Niu; H. Xie; Y. Chen; Y. Yuan; Y. Gao; H. Xiao; J. Tang; A. Pan; B. Yang, Rubidium Doping to Enhance Carrier Transport in Cspbbr3 Single Crystals for High-Performance X-Ray Detection. *ACS Applied Materials & Interfaces* **2020,** *12* (1), 989-996.
[36] C.-C. Hsu; S.-L. Lin; C. A. Chang, Lanthanide-Doped Core–Shell–Shell Nanocomposite for Dual Photodynamic Therapy and Luminescence Imaging by a Single X-Ray Excitation Source. *ACS Applied Materials & Interfaces* **2018**.
[37] T. Kusama; T. Omori; T. Saito; S. Kise; T. Tanaka; Y. Araki; R. Kainuma, Ultra-Large Single Crystals by Abnormal Grain Growth. *Nature Communications* **2017,** *8* (1), 354.
[38] E. I. Gorokhova; G. V. Anan'eva; V. A. Demidenko; P. A. Rodnyĭ; I. V. Khodyuk; E. D. Bourret-Courchesne, Optical, Luminescence, and Scintillation Properties of Zno and Zno:Ga Ceramics. *Journal of Optical Technology* **2008,** *75* (11), 741-746.
[39] W. Chen; J. Zhang, Using Nanoparticles to Enable Simultaneous Radiation and Photodynamic Therapies for Cancer Treatment. *Journal of Nanoscience and Nanotechnology* **2006,** *6* (4), 1159-1166.
[40] R.-P. Jia; G.-X. Zhang; Q.-S. Wu; Y.-P. Ding, $Znwo_4$–Tio_2 Composite Nanofilms: Preparation, Morphology, Structure and Photoluminescent Enhancement. *Materials Letters* **2007,** *61* (8-9), 1793-1797.
[41] S. Sen; M. Tyagi; K. Sharma; P. S. Sarkar; S. Sarkar; C. B. Basak; S. Pitale; M. Ghosh; S. C. Gadkari, Organic–Inorganic Composite Films Based on $Gd_3ga_3al_2o_{12}$:Ce Scintillator Nanoparticles for X-Ray Imaging Applications. *ACS Applied Materials & Interfaces* **2017,** *9* (42), 37310-37320.
[42] Dmitri V. Talapin, †,‡ Jong-Soo Lee,† Maksym V. Kovalenko,† and Elena V. Shevchenko‡, Prospects of Colloidal Nanocrystals for Electronic and Optoelectronic Applications. *Chem. Rev.* **2010,** *110* (1), 389-458.

[43] M. Nikl; A. Yoshikawa, Recent R&D Trends in Inorganic Single-Crystal Scintillator Materials for Radiation Detection. *Advanced Optical Materials* **2015,** *3* (4), 463-481.
[44] P. Schuster; E. Brubaker, Investigating the Anisotropic Scintillation Response in Anthracene through Neutron, Gamma-Ray, and Muon Measurements. *IEEE Transactions on Nuclear Science* **2016,** *63* (3), 1942-1954.
[45] J. Shamsi; A. S. Urban; M. Imran; L. De Trizio; L. Manna, Metal Halide Perovskite Nanocrystals: Synthesis, Post-Synthesis Modifications, and Their Optical Properties. *Chemical Reviews* **2019,** *119* (5), 3296-3348.
[46] Y. Zhang; W. Jie; P. Chen; W. Liu; J. Hao, Ferroelectric and Piezoelectric Effects on the Optical Process in Advanced Materials and Devices. *Advanced Materials* **2018,** *30* (34), 1707007.
[47] H. Zhu; P. Zhang; S. Dai, Recent Advances of Lanthanum-Based Perovskite Oxides for Catalysis. *ACS Catalysis* **2015,** *5* (11), 6370-6385.
[48] Y. Wei; Z. Cheng; J. Lin, An Overview on Enhancing the Stability of Lead Halide Perovskite Quantum Dots and Their Applications in Phosphor-Converted Leds. *Chemical Society Reviews* **2019,** *48* (1), 310-350.
[49] W.-J. Yin; B. Weng; J. Ge; Q. Sun; Z. Li; Y. Yan, Oxide Perovskites, Double Perovskites and Derivatives for Electrocatalysis, Photocatalysis, and Photovoltaics. *Energy & Environmental Science* **2019,** *12* (2), 442-462.
[50] L. Wang; H. Zhou; J. Hu; B. Huang; M. Sun; B. Dong; G. Zheng; Y. Huang; Y. Chen; L. Li; Z. Xu; N. Li; Z. Liu; Q. Chen; L.-D. Sun; C.-H. Yan, A Eu^{3+}-Eu^{2+} Ion Redox Shuttle Imparts Operational Durability to Pb-I Perovskite Solar Cells. *Science* **2019,** *363* (6424), 265-270.
[51] R. Saha; A. Sundaresan; C. N. R. Rao, Novel Features of Multiferroic and Magnetoelectric Ferrites and Chromites Exhibiting Magnetically Driven Ferroelectricity. *Materials Horizons* **2014,** *1* (1), 20-31.
[52] J.-S. Yao; J. Ge; B.-N. Han; K.-H. Wang; H.-B. Yao; H.-L. Yu; J.-H. Li; B.-S. Zhu; J.-Z. Song; C. Chen; Q. Zhang; H.-B. Zeng; Y. Luo; S.-H. Yu, Ce^{3+}-Doping to Modulate Photoluminescence Kinetics for Efficient $Cspbbr_3$ Nanocrystals Based Light-Emitting Diodes. *Journal of the American Chemical Society* **2018,** *140* (10), 3626-3634.
[53] Y. Cheng; C. Shen; L. Shen; W. Xiang; X. Liang, Tb^{3+}, Eu^{3+} Co-Doped $Cspbbr_3$ Qds Glass with Highly Stable and Luminous Adjustable for White Leds. *ACS Applied Materials & Interfaces* **2018,** *10* (25), 21434-21444.
[54] J. Miao; F. Zhang, Recent Progress on Highly Sensitive Perovskite Photodetectors. *Journal of Materials Chemistry C* **2019,** *7* (7), 1741-1791.
[55] T. Addabbo; F. Bertocci; A. Fort; M. Gregorkiewitz; M. Mugnaini; R. Spinicci; V. Vignoli, Gas Sensing Properties of $Ymno_3$ Based Materials for the Detection of Nox and Co. *Sensors and Actuators B: Chemical* **2017,** *244*, 1054-1070.
[56] M. Pellerin; E. Glais; T. Lecuyer; J. Xu; J. Seguin; S. Tanabe; C. Chanéac; B. Viana; C. Richard, $Laalo_3$:Cr^{3+}, Sm^{3+}: Nano-Perovskite with Persistent Luminescence for in Vivo Optical Imaging. *Journal of Luminescence* **2018,** *202*, 83-88.
[57] C. Szeles, Cdznte and Cdte Materials for X-Ray and Gamma Ray Radiation Detector Applications. *physica status solidi (b)* **2004,** *241*, 783-790.
[58] S. O. Kasap; J. A. Rowlands, Direct-Conversion Flat-Panel X-Ray Image Sensors for Digital Radiography. *Proceedings of the IEEE* **2002,** *90* (4), 591-604.
[59] P. Büchele; M. Richter; S. Tedde; G. Matt; G. Ankah; R. Fischer; M. Biele; W. Metzger; S. Lilliu; O. Bikondoa; E. Macdonald; C. Brabec; T. Kraus; U. Lemmer; O. Schmidt, X-Ray Imaging with Scintillator-Sensitized Hybrid Organic Photodetectors. *Nature Photonics* **2015**.

[60] M. Nikl, Scintillation Detectors for X-Rays. *Measurement Science and Technology* **2006,** *17* (4), R37-R54.
[61] M. D. Birowosuto; P. Dorenbos, Novel Γ- and X-Ray Scintillator Research: On the Emission Wavelength, Light Yield and Time Response of Ce3+ Doped Halide Scintillators. *physica status solidi (a)* **2009,** *206* (1), 9-20.
[62] W. Drozdowski; A. Wojtowicz; T. Łukasiewicz; J. Kisielewski, Scintillation Properties of Luap and Luyap Crystals Activated with Cerium and Molybdenum. *Nuclear Instruments and Methods in Physics Research Section A: Accelerators, Spectrometers, Detectors and Associated Equipment* **2006,** *562*, 254-261.
[63] K. Shibuya; M. Koshimizu; Y. Takeoka; K. Asai, Scintillation Properties of $(C_6h_{13}nh_3)_2pbi_4$: Exciton Luminescence of an Organic/Inorganic Multiple Quantum Well Structure Compound Induced by 2.0 Mev Protons. *Nuclear Instruments and Methods in Physics Research Section B: Beam Interactions with Materials and Atoms* **2002,** *194*, 207-212.
[64] S. Kishimoto; K. Shibuya; F. Nishikido; M. Koshimizu; R. Haruki; Y. Yoda, Subnanosecond Time-Resolved X-Ray Measurements Using an Organic-Inorganic Perovskite Scintillator. *Applied Physics Letters* **2008,** *93*, 261901-261901.
[65] F. Cao; D. Yu; W. Ma; X. Xu; B. Cai; Y. M. Yang; S. Liu; L. He; Y. Ke; S. Lan; K.-L. Choy; H. Zeng, Shining Emitter in a Stable Host: Design of Halide Perovskite Scintillators for X-Ray Imaging from Commercial Concept. *ACS Nano* **2020,** *14* (5), 5183-5193.
[66] C. Dujardin; E. Auffray; E. Bourret-Courchesne; P. Dorenbos; P. Lecoq; M. Nikl; A. N. Vasil'ev; A. Yoshikawa; R. Zhu, Needs, Trends, and Advances in Inorganic Scintillators. *IEEE Transactions on Nuclear Science* **2018,** *65* (8), 1977-1997.
[67] S. Khalfin; Y. Bekenstein, Advances in Lead-Free Double Perovskite Nanocrystals, Engineering Band-Gaps and Enhancing Stability through Composition Tunability. *Nanoscale* **2019,** *11* (18), 8665-8679.
[68] N. Phung; A. Abate, The Impact of Nano- and Microstructure on the Stability of Perovskite Solar Cells. *Small* **2018,** *14* (46), 1802573.
[69] X. Wang; T. Hisatomi; Z. Wang; J. Song; J. Qu; T. Takata; K. Domen, Core–Shell-Structured $Lataon_2$ Transformed from $Laknatao_5$ Plates for Enhanced Photocatalytic H_2 Evolution. *Angewandte Chemie International Edition* **2019,** *58* (31), 10666-10670.
[70] G. Pan; X. Bai; D. Yang; X. Chen; P. Jing; S. Qu; L. Zhang; D. Zhou; J. Zhu; W. Xu; B. Dong; H. Song, Doping Lanthanide into Perovskite Nanocrystals: Highly Improved and Expanded Optical Properties. *Nano Letters* **2017,** *17* (12), 8005-8011.
[71] M. A. Becker; R. Vaxenburg; G. Nedelcu; P. C. Sercel; A. Shabaev; M. J. Mehl; J. G. Michopoulos; S. G. Lambrakos; N. Bernstein; J. L. Lyons; T. Stöferle; R. F. Mahrt; M. V. Kovalenko; D. J. Norris; G. Rainò; A. L. Efros, Bright Triplet Excitons in Caesium Lead Halide Perovskites. *Nature* **2018,** *553* (7687), 189-193.
[72] F. Hu; H. Zhang; C. Sun; C. Yin; B. Lv; C. Zhang; W. W. Yu; X. Wang; Y. Zhang; M. Xiao, Superior Optical Properties of Perovskite Nanocrystals as Single Photon Emitters. *ACS Nano* **2015,** *9* (12), 12410-6.
[73] Y. Zhang; R. Sun; X. Ou; K. Fu; Q. Chen; Y. Ding; L.-J. Xu; L. Liu; Y. Han; A. V. Malko; X. Liu; H. Yang; O. M. Bakr; H. Liu; O. F. Mohammed, Metal Halide Perovskite Nanosheet for X-Ray High-Resolution Scintillation Imaging Screens. *ACS Nano* **2019,** *13* (2), 2520-2525.
[74] L. Wang; K. Fu; R. Sun; H. Lian; X. Hu; Y. Zhang, Ultra-Stable Cspbbr3 Perovskite Nanosheets for X-Ray Imaging Screen. *Nano-Micro Letters* **2019,** *11* (1), 52.

[75] L. Lian; M. Zheng; W. Zhang; L. Yin; X. Du; P. Zhang; X. Zhang; J. Gao; D. Zhang; L. Gao; G. Niu; H. Song; R. Chen; X. Lan; J. Tang; J. Zhang, Efficient and Reabsorption-Free Radioluminescence in Cs3cu2i5 Nanocrystals with Self-Trapped Excitons. *Advanced Science* **2020,** *7* (11), 2000195.
[76] J. Duan; J. Wei; Q. Tang; Q. Li, Unveiling the Interfacial Charge Extraction Kinetics in Inorganic Perovskite Solar Cells with Formamidinium Lead Halide (Fapbx3) Nanocrystals. *Solar Energy* **2020,** *195*, 644-650.
[77] C. Zheng; C. Bi; F. Huang; D. Binks; J. Tian, Stable and Strong Emission $Cspbbr_3$ Quantum Dots by Surface Engineering for High-Performance Optoelectronic Films. *ACS Applied Materials & Interfaces* **2019,** *11* (28), 25410-25416.
[78] M. D. Smith; B. A. Connor; H. I. Karunadasa, Tuning the Luminescence of Layered Halide Perovskites. *Chemical Reviews* **2019,** *119* (5), 3104-3139.
[79] W. Xiang; Z. Wang; D. J. Kubicki; W. Tress; J. Luo; D. Prochowicz; S. Akin; L. Emsley; J. Zhou; G. Dietler; M. Grätzel; A. Hagfeldt, Europium-Doped $Cspbi_2br$ for Stable and Highly Efficient Inorganic Perovskite Solar Cells. *Joule* **2019,** *3* (1), 205-214.
[80] Z. Zeng; Y. Xu; Z. Zhang; Z. Gao; M. Luo; Z. Yin; C. Zhang; J. Xu; B. Huang; F. Luo; Y. Du; C. Yan, Rare-Earth-Containing Perovskite Nanomaterials: Design, Synthesis, Properties and Applications. *Chem Soc Rev* **2020,** *49* (4), 1109-1143.
[81] W. W. Moses, Time of Flight in Pet Revisited. *IEEE Transactions on Nuclear Science* **2003,** *50* (5), 1325-1330.
[82] C. W. E. van Eijk, Inorganic-Scintillator Development. *Nuclear Instruments and Methods in Physics Research Section A: Accelerators, Spectrometers, Detectors and Associated Equipment* **2001,** *460* (1), 1-14.
[83] N. Kawano; M. Koshimizu; G. Okada; Y. Fujimoto; N. Kawaguchi; T. Yanagida; K. Asai, Scintillating Organic–Inorganic Layered Perovskite-Type Compounds and the Gamma-Ray Detection Capabilities. *Scientific Reports* **2017,** *7* (1).
[84] K. Shibuya; M. Koshimizu; Y. Takeoka; K. Asai, Scintillation Properties of (C6h13nh3)2pbi4: Exciton Luminescence of an Organic/Inorganic Multiple Quantum Well Structure Compound Induced by 2.0 Mev Protons. *Nuclear Instruments and Methods in Physics Research Section B: Beam Interactions with Materials and Atoms* **2002,** *194* (2), 207-212.
[85] N. Kawano; M. Koshimizu; G. Okada; Y. Fujimoto; N. Kawaguchi; T. Yanagida; K. Asai, Scintillating Organic–Inorganic Layered Perovskite-Type Compounds and the Gamma-Ray Detection Capabilities. *Scientific Reports* **2017,** *7* (1), 14754.
[86] U. Shirwadkar; E. V. v. Loef; G. Markosyan; M. McClish; J. Glodo; K. S. Shah; P. L. Feng; N. Myllenbeck; R. Dhaoui In *Progress on Metal-Loaded Plastic Scintillators for Nuclear Security Applications*, 2017 IEEE Nuclear Science Symposium and Medical Imaging Conference (NSS/MIC), 21-28 Oct. 2017; 2017; pp 1-3.
[87] Z. Zheng; Y. Tong; R. Wei; F. Hu; X. Sun; H. Guo, Tb^{3+} -Doped Transparent $Bagdf_5$ Glass-Ceramics Scintillator for X-Ray Detector. *Journal of the American Ceramic Society* **2019**.
[88] X. Chen; J. Song; X. Chen; H. Yang, X-Ray-Activated Nanosystems for Theranostic Applications. *Chemical Society Reviews* **2019,** *48* (11), 3073-3101.
[89] Z. Du; X. Zhang; Z. Guo; J. Xie; X. Dong; S. Zhu; J. Du; Z. Gu; Y. Zhao, X-Ray-Controlled Generation of Peroxynitrite Based on Nanosized $Liluf_4$:Ce^{3+} Scintillators and Their Applications for Radiosensitization. *Advanced Materials* **2018,** *30* (43), 1804046.

[90] A. Kamkaew; F. Chen; Y. Zhan; R. L. Majewski; W. Cai, Scintillating Nanoparticles as Energy Mediators for Enhanced Photodynamic Therapy. *ACS Nano* **2016,** *10* (4), 3918-3935.
[91] G. F. Knoll, Radiation Detection and Measurement. *Wiley, New York* **2000**.
[92] K. Yang; P. R. Menge; J. J. Buzniak; V. Ouspenski In *Performance Improvement of Large Sr^{2+} and Ba^{2+} Co-Doped $Labr_3:Ce^{3+}$ Scintillation Crystals*, 2012 IEEE Nuclear Science Symposium and Medical Imaging Conference Record (NSS/MIC), 27 Oct.-3 Nov. 2012; 2012; pp 308-311.
[93] B. W. Sturm; N. J. Cherepy; O. B. Drury; P. A. Thelin; S. E. Fisher; S. A. Payne; A. Burger; L. A. Boatner; J. O. Ramey; K. S. Shah; R. Hawrami, Effects of Packaging Sri_2(Eu) Scintillator Crystals. *Nuclear Instruments and Methods in Physics Research Section A: Accelerators, Spectrometers, Detectors and Associated Equipment* **2011,** *652* (1), 242-246.
[94] M. Rozler; H. Liang; H. Sabet; W. Chang, Development of a Cost-Effective Modular Pixelated Nai(Tl) Detector for Clinical Spect Applications. *IEEE Transactions on Nuclear Science* **2012,** *59* (5), 1831-1840.
[95] I. Valais; C. Michail; S. David; C. D. Nomicos; G. S. Panayiotakis; I. Kandarakis, A Comparative Study of the Luminescence Properties of Lyso:Ce, Lso:Ce, Gso:Ce and Bgo Single Crystal Scintillators for Use in Medical X-Ray Imaging. *Physica Medica* **2008,** *24* (2), 122-125.
[96] F. Maddalena; L. Tjahjana; A. Xie; Arramel; S. Zeng; H. Wang; P. Coquet; W. Drozdowski; C. Dujardin; C. Dang; M. Birowosuto, Inorganic, Organic, and Perovskite Halides with Nanotechnology for High–Light Yield X- and Γ-Ray Scintillators. *Crystals* **2019,** *9* (2).
[97] E. Sysoeva; V. Tarasov; O. Zelenskaya, Comparison of the Methods for Determination of Scintillation Light Yield. *Nuclear Instruments and Methods in Physics Research Section A: Accelerators, Spectrometers, Detectors and Associated Equipment* **2002,** *486* (1), 67-73.
[98] A. Lempicki; A. J. Wojtowicz; E. Berman, Fundamental Limits of Scintillator Performance. *Nuclear Instruments and Methods in Physics Research Section A: Accelerators, Spectrometers, Detectors and Associated Equipment* **1993,** *333* (2), 304-311.
[99] M. Moszyński; A. Syntfeld-Każuch; L. Swiderski; M. Grodzicka; J. Iwanowska; P. Sibczyński; T. Szczęśniak, Energy Resolution of Scintillation Detectors. *Nuclear Instruments and Methods in Physics Research Section A: Accelerators, Spectrometers, Detectors and Associated Equipment* **2016,** *805*, 25-35.
[100] S. E. Derenzo; M. J. Weber; E. Bourret-Courchesne; M. K. Klintenberg, The Quest for the Ideal Inorganic Scintillator. *Nuclear Instruments and Methods in Physics Research Section A: Accelerators, Spectrometers, Detectors and Associated Equipment* **2003,** *505* (1-2), 111-117.
[101] J.-R. L. Fa-Xin Yu, Zheng-Liang Huang, Hao Luo, Zhe-Ming Lu, Overview of Radiation Hardening Techniques for Ic Design. . *Information Technology Journal* **2010,** *9* (6), 1068-1080.
[102] Z. Lei; C. Zhu; C. Xu; B. Yao; C. Yang, Growth of Crack-Free Zngep2 Large Single Crystals for High-Power Mid-Infrared Opo Applications. *Journal of Crystal Growth* **2014,** *389*, 23-29.
[103] N. Ye; J. Y. Wang; R. I. Boughton; M. C. Hong, Chapter 20 - Functional Crystals. In *Modern Inorganic Synthetic Chemistry (Second Edition)*, Xu, R.; Xu, Y., Eds. Elsevier: Amsterdam, 2017; pp 575-611.

[104] W. Huda; R. B. Abrahams, X-Ray-Based Medical Imaging and Resolution. *American Journal of Roentgenology* **2015,** *204* (4), W393-W397.
[105] P. Lecoq, Development of New Scintillators for Medical Applications. *Nuclear Instruments and Methods in Physics Research Section A: Accelerators, Spectrometers, Detectors and Associated Equipment* **2016,** *809*, 130-139.
[106] K. Van den Eeckhout; P. F. Smet; D. Poelman, Persistent Luminescence in Eu^{2+}-Doped Compounds: A Review. *Materials* **2010,** *3* (4), 2536.
[107] K. Van den Eeckhout; D. Poelman; P. Smet, Persistent Luminescence in Non-Eu^{2+}-Doped Compounds: A Review. *Materials* **2013,** *6* (7), 2789.
[108] P. F. Smet; I. Moreels; Z. Hens; D. Poelman, Luminescence in Sulfides: A Rich History and a Bright Future. *Materials* **2010,** *3* (4), 2834.
[109] J. Hölsä, Persistent Luminescence Beats the Afterglow: 400 Years of Persistent Luminescence. *Electrochem. Soc. Interf.* **2009,** *18*, 42-45.
[110] M. Sun; H. Dong; A. W. Dougherty; Q. Lu; D. Peng; W.-T. Wong; B. Huang; L.-D. Sun; C.-H. Yan, Nanophotonic Energy Storage in Upconversion Nanoparticles. *Nano Energy* **2019,** *56*, 473-481.
[111] H. Yamada; A. Suzuki; Y. Uchida; M. Yoshida; Y. Tsukuda, Cheminform Abstract: A Scintillator Gd2o2s:Pr, Ce, F for X-Ray Computed Tomography. *J. Electrochem. Soc* **1990,** *136* (9), 2713-2716.
[112] G. Blasse, Scintillator Materials. *Chemistry of Materials* **1994,** *6* (9), 1465-1475.
[113] C. W. E. van Eijk, Fast Scintillators and Their Applications. *Nuclear Tracks and Radiation Measurements* **1993,** *21* (1), 5-10.
[114] C. W. E. v. Eijk; P. Dorenbos; R. Visser, Nd/Sup 3+/ and Pr/Sup 3+/ Doped Inorganic Scintillators. *IEEE Transactions on Nuclear Science* **1994,** *41* (4), 738-741.
[115] P. A. Rodnyi; P. Dorenbos; C. W. E. van Eijk, Energy Loss in Inorganic Scintillators. *physica status solidi (b)* **1995,** *187* (1), 15-29.
[116] P. Dorenbos, Scintillation Mechanisms in Ce^{3+} Doped Halide Scintillators. *physica status solidi (a)* **2005,** *202* (2), 195-200.
[117] H. Hall, The Theory of Photoelectric Absorption for X-Rays and $¥Ensuremath{¥Gamma}$-Rays. *Reviews of Modern Physics* **1936,** *8* (4), 358-397.
[118] P. Eisenberger; P. M. Platzman, Compton Scattering of X Rays from Bound Electrons. *Physical Review A* **1970,** *2* (2), 415-423.
[119] J. H. Hubbell, Electron–Positron Pair Production by Photons: A Historical Overview. *Radiation Physics and Chemistry* **2006,** *75* (6), 614-623.
[120] G. H. Kinchin; R. S. Pease, The Displacement of Atoms in Solids by Radiation. *Reports on Progress in Physics* **1955,** *18* (1), 1-51.
[121] J. Frenkel, Über Die Wärmebewegung in Festen Und Flüssigen Körpern. *Zeitschrift für Physik* **1926,** *35* (8), 652-669.
[122] D. P. Karim; A. T. Aldred, Localized Level Hopping Transport in La(Sr)Cr${¥Mathrm{O}}_{3}$. *Physical Review B* **1979,** *20* (6), 2255-2263.
[123] A. S. John; M. G. Sol; W. T. Mark; T. Melvin, Study of Afterglow in X-Ray Phosphors for Use on Fast-Framing Charge-Coupled Device Detectors. *Optical Engineering* **1997,** *36* (11), 3212-3222.
[124] G. Blasse, New Luminescent Materials. *Chemistry of Materials* **1989,** *1* (3), 294-301.
[125] D. S. McGregor, Materials for Gamma-Ray Spectrometers: Inorganic Scintillators. *Annual Review of Materials Research* **2018,** *48* (1), 245-277.

[126] H. Luo; A. J. J. Bos; P. Dorenbos, Controlled Electron–Hole Trapping and Detrapping Process in $Gdalo_3$ by Valence Band Engineering. *The Journal of Physical Chemistry C* **2016,** *120* (11), 5916-5925.
[127] P. Dorenbos, Electronic Structure Engineering of Lanthanide Activated Materials. *Journal of Materials Chemistry* **2012,** *22* (42), 22344-22349.
[128] Y. Wu; Q. Li; S. Jones; C. Dun; S. Hu; M. Zhuravleva; A. C. Lindsey; L. Stand; M. Loyd; M. Koschan; J. Auxier; H. L. Hall; C. L. Melcher, Defect Engineeringby Codopingin $Kcai_3:Eu^{2+}$Single-Crystalline Scintillators. *Physical Review Applied* **2017,** *8* (3), 034011.
[129] M. S. Alekhin; J. T. M. de Haas; I. V. Khodyuk; K. W. Kra?mer; P. R. Menge; V. Ouspenski; P. Dorenbos, Improvement of Γ-Ray Energy Resolution of $Labr_3:Ce^{3+}$ Scintillation Detectors by Sr^{2+} and Ca^{2+} Co-Doping. *Applied Physics Letters* **2013,** *102* (16), 161915.
[130] Lin; E. C., Radiation Risk from Medical Imaging. *Mayo Clinic Proceedings* **2010,** *85* (12), 1142-1146.
[131] H. Wei; Y. Fang; P. Mulligan; W. Chuirazzi; H.-H. Fang; C. Wang; B. R. Ecker; Y. Gao; M. A. Loi; L. Cao; J. Huang, Sensitive X-Ray Detectors Made of Methylammonium Lead Tribromide Perovskite Single Crystals. *Nature Photonics* **2016,** *10* (5), 333-339.
[132] W. Heiss; C. Brabec, Perovskites Target X-Ray Detection. *Nature Photonics* **2016,** *10* (5), 288-289.
[133] S. O. Kasap, X-Ray Sensitivity of Photoconductors: Application to Stabilized a-Se. *Journal of Physics D: Applied Physics* **2000,** *33* (21), 2853-2865.
[134] K. Kobayashi; N. Usami; E. Porcel; S. Lacombe; C. L. Sech, Enhancement of Radiation Effect by Heavy Elements. *Mutation Research/reviews in Mutation Research* **2010,** *704* (1-3), 123-131.
[135] I. M. Band; Y. I. Kharitonov; M. B. Trzhaskovskaya, Photoionization Cross Sections and Photoelectron Angular Distributions for X-Ray Line Energies in the Range 0.132–4.509 Kev Targets: $1 \leq Z \leq 100$. **1979,** *23* (5), 443-505.
[136] D. R. Cooper; D. Bekah; J. L. Nadeau, Gold Nanoparticles and Their Alternatives for Radiation Therapy Enhancement. *Front Chem* **2014,** *2*, 86.
[137] P.; Schotanus; and; C.W.E.; Van; Eijk; and; R.W.; Hollander, Detection of $Laf_3:Nd^{3+}$ Scintillation Light in a Photosensitive Multiwire Chamber. *Nuclear Instruments and Methods in Physics Research Section A: Accelerators, Spectrometers, Detectors and Associated Equipment* **1988,** *272* (3), 913-916.
[138] J. A. Mareš; B. Jacquier; C. Pédrini; G. Boulon, Fluorescence Decays and Lifetimes of Nd^{3+}, Ce^{3+} and Cr^{3+} in Yag. *Czechoslovak Journal of Physics B* **1988,** *38* (7), 802-816.
[139] P. Dorenbos, (Invited) the Quest for High Resolution Γ-Ray Scintillators. *Optical Materials: X* **2019,** *1*.
[140] N. J. P. Cherepy, S.A.; Asztalos, S.J.; Hull, G.; Kuntz, J.D.; Niedermayr, T.; Pimputkar, S.; Roberts, J.J.;; R. D. T. Sanner, T.M.; et al., Scintillators with Potential to Supersede Lanthanum Bromide. *IEEE Transactions on Nuclear Science* **2009,** *56* (3), 873-880.
[141] M. D. Birowosuto; P. Dorenbos; C. W. E. V. Eijk; K. W. Krämer; H. U. Güdel, Thermal Quenching of Ce^{3+} Emission in Prx_3 (X = Cl, Br) by Intervalence Charge Transfer. *Journal of Physics Condensed Matter* **2007,** *19* (25), 256209.
[142] Y. Osakada; G. Pratx; L. Hanson; P. E. Solomon; L. Xing; B. Cui, X-Ray Excitable Luminescent Polymer Dots Doped with an Iridium(Iii) Complex. *Chemical Communications* **2013,** *49* (39), 4319-4321.

[143] W. Chen, Nanoparticle Self-Lighting Photodynamic Therapy for Cancer Treatment. *Journal of Biomedical Nanotechnology* **2008,** *4* (4), 369-376.
[144] T. Y. Elmenoufy AH, Hu J, Xu H, Yang X, A Novel Deep Photodynamic Therapy Modality Combined with Ct Imaging Established Via X-Ray Stimulated Silica-Modified Lanthanide Scintillating Nanoparticles. *Chemical Communications* **2015,** *51* (61), 12247-12250.
[145] D. C. Rodriguez Burbano; E. M. Rodriguez; P. Dorenbos; M. Bettinelli; J. A. Capobianco, The near-Ir Photo-Stimulated Luminescence of Cas:Eu^{2+}/Dy^{3+} Nanophosphors. *Journal of Materials Chemistry C* **2014,** *2* (2), 228-231.
[146] L. Song; X. H. Lin; X. R. Song; S. Chen; X. F. Chen; J. Li; H. H. Yang, Repeatable Deep-Tissue Activation of Persistent Luminescent Nanoparticles by Soft X-Ray for High Sensitivity Long-Term in Vivo Bioimaging. *Nanoscale* **2017,** *9* (8), 2718-2722.
[147] H. Dong; S.-R. Du; X.-Y. Zheng; G.-M. Lyu; L.-D. Sun; L.-D. Li; P.-Z. Zhang; C. Zhang; C.-H. Yan, Lanthanide Nanoparticles: From Design toward Bioimaging and Therapy. *Chemical Reviews* **2015,** *115* (19), 10725-10815.
[148] Y. Wu; G. Ren; F. Meng; X. Chen; D. Ding; H. Li; S. Pan, Ultralow-Concentration Sm Codoping in Csi:Tl Scintillator: A Case of Little Things Can Make a Big Difference. *Optical Materials* **2014,** *38*, 297-300.
[149] W. Van Sciver; R. Hofstadter, Scintillations in Thallium-Activated Cai_2 and Csi. *Physical Review* **1951,** *84* (5), 1062-1063.
[150] J. H. Siewerdsen; D. A. Jaffray, A Ghost Story: Spatio-Temporal Response Characteristics of an Indirect- Detection Flat-Panel Imager. *Medical Physics* **1999,** *26* (8), 1624-1641.
[151] P. G. Jung; C. H. Lee; K. M. Bae; J. M. Lee; S. M. Lee; C. H. Lim; S. Yun; H. K. Kim; J. S. Ko, Microdome-Gooved Gd_2o_2s:Tb Scintillator for Flexible and High Resolution Digital Radiography. **2010,** *18* (14), 14850.
[152] I. Jung; M. Cho; S. Lee; K. Bae; P. Jung; C. Lee; J. Lee; S. Yun; H. K. Kim; S. Kim; J. Ko, Flexible Gd_2o_2s:Tb Scintillators Pixelated with Polyethylene Microstructures for Digital X-Ray Image Sensors. *Journal of Micromechanics and Microengineering* **2008,** *19*, 015014.
[153] X. Badel; A. Galeckas; J. Linnros; P. Kleimann; C. Fröjdh; C. S. Petersson, Improvement of an X-Ray Imaging Detector Based on a Scintillating Guides Screen. *Nuclear Instruments and Methods in Physics Research Section A: Accelerators, Spectrometers, Detectors and Associated Equipment* **2002,** *487* (1), 129-135.
[154] M. Simon; K. J. Engel; B. Menser; X. Badel; J. Linnros, X-Ray Imaging Performance of Scintillator-Filled Silicon Pore Arrays. *Medical Physics* **2008,** *35* (3), 968-981.
[155] F. Cao; D. Yu; W. Ma; X. Xu; B. Cai; Y. M. Yang; S. Liu; L. He; Y. Ke; S. Lan; K. L. Choy; H. Zeng, Shining Emitter in a Stable Host: Design of Halide Perovskite Scintillators for X-Ray Imaging from Commercial Concept. *ACS Nano* **2019**.
[156] Y. Li; W. Shao; X. Ouyang; Z. Zhu; H. Zhang; X. Ouyang; B. Liu; Q. Xu, Scintillation Properties of Perovskite Single Crystals. *The Journal of Physical Chemistry C* **2019,** *123* (28), 17449-17453.
[157] S. Yakunin; M. Sytnyk; D. Kriegner; S. Shrestha; M. Richter; G. J. Matt; H. Azimi; C. J. Brabec; J. Stangl; M. V. Kovalenko; W. Heiss, Detection of X-Ray Photons by Solution-Processed Lead Halide Perovskites. *Nature Photonics* **2015,** *9* (7), 444-449.
[158] X. Y. Chin; D. Cortecchia; J. Yin; A. Bruno; C. Soci, Lead Iodide Perovskite Light-Emitting Field-Effect Transistor. *Nature Communications* **2015,** *6* (1), 7383.

[159] K. Chondroudis; D. B. Mitzi, Electroluminescence from an Organic−Inorganic Perovskite Incorporating a Quaterthiophene Dye within Lead Halide Perovskite Layers. *Chemistry of Materials* **1999,** *11* (11), 3028-3030.
[160] Z.-K. Tan; R. S. Moghaddam; M. L. Lai; P. Docampo; R. Higler; F. Deschler; M. Price; A. Sadhanala; L. M. Pazos; D. Credgington; F. Hanusch; T. Bein; H. J. Snaith; R. H. Friend, Bright Light-Emitting Diodes Based on Organometal Halide Perovskite. *Nature Nanotechnology* **2014,** *9* (9), 687-692.
[161] L. Dou; Y. Yang; J. You; Z. Hong; W.-H. Chang; G. Li; Y. Yang, Solution-Processed Hybrid Perovskite Photodetectors with High Detectivity. *Nature Communications* **2014,** *5* (1), 5404.
[162] M. I. Saidaminov; A. L. Abdelhady; B. Murali; E. Alarousu; V. M. Burlakov; W. Peng; I. Dursun; L. Wang; Y. He; G. Maculan; A. Goriely; T. Wu; O. F. Mohammed; O. M. Bakr, High-Quality Bulk Hybrid Perovskite Single Crystals within Minutes by Inverse Temperature Crystallization. *Nature Communications* **2015,** *6* (1), 7586.
[163] D. Shi; V. Adinolfi; R. Comin; M. Yuan; E. Alarousu; A. Buin; Y. Chen; S. Hoogland; A. Rothenberger; K. Katsiev; Y. Losovyj; X. Zhang; P. A. Dowben; O. F. Mohammed; E. H. Sargent; O. M. Bakr, Low Trap-State Density and Long Carrier Diffusion in Organolead Trihalide Perovskite Single Crystals. *Science* **2015,** *347* (6221), 519.
[164] E. R. Dohner; A. Jaffe; L. R. Bradshaw; H. I. Karunadasa, Intrinsic White-Light Emission from Layered Hybrid Perovskites. *Journal of the American Chemical Society* **2014,** *136* (38), 13154-13157.
[165] W. Drozdowski; A. J. Wojtowicz; T. Łukasiewicz; J. Kisielewski, Scintillation Properties of Luap and Luyap Crystals Activated with Cerium and Molybdenum. *Nuclear Instruments and Methods in Physics Research Section A: Accelerators, Spectrometers, Detectors and Associated Equipment* **2006,** *562* (1), 254-261.
[166] W. Drozdowski; K. Brylew; M. E. Witkowski; A. J. Wojtowicz; P. Solarz; K. Kamada; A. Yoshikawa, Studies of Light Yield as a Function of Temperature and Low Temperature Thermoluminescence of Gd3al2ga3o12:Ce Scintillator Crystals. *Optical Materials* **2014,** *36* (10), 1665-1669.
[167] T. Yanagida; Y. Fujimoto; T. Ito; K. Uchiyama; K. Mori, Development of X-Ray-Induced Afterglow Characterization System. *Applied Physics Express* **2014,** *7* (6), 062401.
[168] E. van der Kolk; P. Dorenbos, Systematic and Material Independent Variation of Electrical, Optical, and Chemical Properties of Ln Materials over the Ln Series (Ln = La, Ce, Pr, ..., Lu). *Chemistry of Materials* **2006,** *18* (15), 3458-3462.
[169] V. V. Nagarkar; T. K. Gupta; S. Miller; Y. Klugarman; G. Entine In *Structured Csi(Tl) Scintillators for X-Ray Imaging Applications*, Nuclear Science Symposium, 1997. IEEE, 1998.
[170] S. Baccaro; K. Bla?ek; F. d. Notaristefani; P. Maly; J. A. Mares; R. Pani; R. Pellegrini; A. Soluri, Scintillation Properties of Yap:Ce. *Nuclear Instruments & Methods in Physics Research* **1995,** *361* (1-2), 209-215.
[171] A. Swarnkar; A. R. Marshall; E. M. Sanehira; B. D. Chernomordik; D. T. Moore; J. A. Christians; T. Chakrabarti; J. M. Luther, Quantum Dot-Induced Phase Stabilization of A-Cspbi3 Perovskite for High-Efficiency Photovoltaics. *Science* **2016,** *354* (6308), 92-95.
[172] P. Schotanus; R. Kamermans, Scintillation Characteristics of Pure and Tl-Doped Csi Crystals. *IEEE Transactions on Nuclear Science* **1990,** *37* (2), 177-182.

[173] C. W. E. v. Eijk, Inorganic Scintillators in Medical Imaging. *Physics in Medicine and Biology* **2002,** *47* (8), R85-R106.
[174] B. Yang; L. Yin; G. Niu; J. H. Yuan; K. H. Xue; Z. Tan; X. S. Miao; M. Niu; X. Du; H. Song; E. Lifshitz; J. Tang, Lead-Free Halide Rb_2cubr_3 as Sensitive X-Ray Scintillator. *Adv Mater* **2019,** *31* (44), e1904711.
[175] M. Liu; G. Zhong; Y. Yin; J. Miao; K. Li; C. Wang; X. Xu; C. Shen; H. Meng, Aluminum-Doped Cesium Lead Bromide Perovskite Nanocrystals with Stable Blue Photoluminescence Used for Display Backlight. *Advanced Science* **2017,** *4* (11), 1700335.
[176] R. T. W. K. Song, *Self-Trapped Excitons*. Springer: Berlin, Heidelberg, 2013; Vol. 105, p 121-127.
[177] F. Di Stasio; S. Christodoulou; N. Huo; G. Konstantatos, Near-Unity Photoluminescence Quantum Yield in Cspbbr3 Nanocrystal Solid-State Films Via Postsynthesis Treatment with Lead Bromide. *Chemistry of Materials* **2017,** *29* (18), 7663-7667.
[178] N. Mondal; A. De; A. Samanta, Achieving near-Unity Photoluminescence Efficiency for Blue-Violet-Emitting Perovskite Nanocrystals. *ACS Energy Letters* **2019,** *4* (1), 32-39.
[179] J. Luo; X. Wang; S. Li; J. Liu; Y. Guo; G. Niu; L. Yao; Y. Fu; L. Gao; Q. Dong; C. Zhao; M. Leng; F. Ma; W. Liang; L. Wang; S. Jin; J. Han; L. Zhang; J. Etheridge; J. Wang; Y. Yan; E. H. Sargent; J. Tang, Efficient and Stable Emission of Warm-White Light from Lead-Free Halide Double Perovskites. *Nature* **2018,** *563* (7732), 541-545.
[180] J. Zhang; Y. Yang; H. Deng; U. Farooq; X. Yang; J. Khan; J. Tang; H. Song, High Quantum Yield Blue Emission from Lead-Free Inorganic Antimony Halide Perovskite Colloidal Quantum Dots. *ACS Nano* **2017,** *11* (9), 9294-9302.
[181] S. Tanaka; T. Nishio; M. Tsuneda; K. Matsushita; S. Kabuki; M. Uesaka, Improved Proton Ct Imaging Using a Bismuth Germanium Oxide Scintillator. *Physics in Medicine & Biology* **2018,** *63* (3), 035030.
[182] Z. Xia; A. Meijerink, Ce^{3+}-Doped Garnet Phosphors: Composition Modification, Luminescence Properties and Applications. *Chemical Society Reviews* **2017,** *46* (1), 275-299.
[183] C. Buck; M. Yeh, Metal-Loaded Organic Scintillators for Neutrino Physics. *Journal of Physics G: Nuclear and Particle Physics* **2016,** *43* (9), 093001.
[184] Y. N. Kharzheev, Scintillation Counters in Modern High-Energy Physics Experiments (Review). *Physics of Particles and Nuclei* **2015,** *46* (4), 678-728.
[185] J. J. Perry Iv; P. L. Feng; S. T. Meek; K. Leong; F. P. Doty; M. D. Allendorf, Connecting Structure with Function in Metal–Organic Frameworks to Design Novel Photo- and Radioluminescent Materials. *Journal of Materials Chemistry* **2012,** *22* (20), 10235-10248.
[186] J. Lu; X.-H. Xin; Y.-J. Lin; S.-H. Wang; J.-G. Xu; F.-K. Zheng; G.-C. Guo, Efficient X-Ray Scintillating Lead(Ii)-Based Mofs Derived from Rigid Luminescent Naphthalene Motifs. *Dalton Transactions* **2019,** *48* (5), 1722-1731.
[187] S. R. Mathis Ii; S. T. Golafale; J. Bacsa; A. Steiner; C. W. Ingram; F. P. Doty; E. Auden; K. Hattar, Mesoporous Stilbene-Based Lanthanide Metal Organic Frameworks: Synthesis, Photoluminescence and Radioluminescence Characteristics. *Dalton Transactions* **2017,** *46* (2), 491-500.
[188] Y. Wang; X. Yin; W. Liu; J. Xie; J. Chen; M. A. Silver; D. Sheng; L. Chen; J. Diwu; N. Liu; Z. Chai; T. E. Albrecht-Schmitt; S. Wang, Emergence of Uranium as a Distinct Metal Center for Building Intrinsic X-Ray Scintillators. *Angewandte Chemie International Edition* **2018,** *57* (26), 7883-7887.

[189] T. Y. Hu J, Elmenoufy AH, Xu H, Cheng Z, Yang X., Nanocomposite-Based Photodynamic Therapy Strategies for Deep Tumor Treatment. *Small* **2015,** *11* (44), 5860-5887.
[190] S. S. Lucky; K. C. Soo; Y. Zhang, Nanoparticles in Photodynamic Therapy. *Chemical Reviews* **2015,** *115* (4), 1990-2042.
[191] C. Zhang; K. Zhao; W. Bu; D. Ni; Y. Liu; J. Feng; J. Shi, Marriage of Scintillator and Semiconductor for Synchronous Radiotherapy and Deep Photodynamic Therapy with Diminished Oxygen Dependence. *Angewandte Chemie International Edition* **2015,** *54* (6), 1770-1774.
[192] Nikl; Martin, Scintillation Detectors for X-Rays. *Measurement Science & Technology* **2006,** *17* (4), 37-54.
[193] W. Sun; Z. Zhou; G. Pratx; X. Chen; H. Chen, Nanoscintillator-Mediated X-Ray Induced Photodynamic Therapy for Deep-Seated Tumors: From Concept to Biomedical Applications. *Theranostics* **2020,** *10* (3), 1296-1318.
[194] W. Chen; J. Zhang, Using Nanoparticles to Enable Simultaneous Radiation and Photodynamic Therapies for Cancer Treatment. *J Nanosci Nanotechnol* **2006,** *6* (4), 1159-1166.
[195] P. Lecoq; A. Annenkov; A. Gektin; M. Korzhik; C. Pedrini, Inorganic Scintillators for Detector Systems: Physical Principles and Crystal Engineering. Berlin, Heidelberg, 2006.
[196] B. Huang; R. Gillen; J. Robertson, Study of Ceo_2 and Its Native Defects by Density Functional Theory with Repulsive Potential. *The Journal of Physical Chemistry C* **2014,** *118* (42), 24248-24256.
[197] M. Sun; Q. He; X. Kuang; Q. Zhang; S. Ye; B. Huang, Probing Oxide-Ion Conduction in Low-Temperature Sofcs. *Nano Energy* **2018,** *50*, 88-96.
[198] J. Barranco; A. Méndez-Blas; M. E. Calixto, Structural, Morphology and Optical Properties of Nayf4 Thin Films Doped with Trivalent Lanthanide Ions. *Journal of Materials Science: Materials in Electronics* **2019,** *30* (5), 4855-4866.
[199] M. Sun; B. Huang, "Energy Selection Channels" for High-Performance Electrolyte: Anion-Frenkel Defect Pair as Dominant Source for O Ion Conductions in Pyrochlore-Type Lanthanide Hafnium Oxides Sofc. *Inorg Chem* **2017,** *56* (14), 7975-7984.
[200] J. Wang; S. Bai; H. Zhang; C. Zhang, The Structure, Thermal Expansion Coefficient and Sintering Behavior of Nd3+-Doped La2zr2o7 for Thermal Barrier Coatings. *J Alloys Compd* **2009,** *476* (1-2), 89-91.
[201] H. Dong; L.-D. Sun; Y.-F. Wang; J. Ke; R. Si; J.-W. Xiao; G.-M. Lyu; S. Shi; C.-H. Yan, Efficient Tailoring of Upconversion Selectivity by Engineering Local Structure of Lanthanides in Na_xref_{3+X} Nanocrystals. *J Am Chem Soc* **2015,** *137* (20), 6569-6576.
[202] J. Xie; Y. Wang; W. Liu; X. Yin; L. Chen; Y. Zou; J. Diwu; Z. Chai; T. E. Albrecht-Schmitt; G. Liu; S. Wang, Highly Sensitive Detection of Ionizing Radiations by a Photoluminescent Uranyl Organic Framework. *Angewandte Chemie International Edition* **2017,** *56* (26), 7500-7504.
[203] J.-B. Li; H.-W. Liu; T. Fu; R. Wang; X.-B. Zhang; W. Tan, Recent Progress in Small-Molecule near-Ir Probes for Bioimaging. *Trends in Chemistry* **2019,** *1* (2), 224-234.
[204] A. M. Smith; M. C. Mancini; S. Nie, Second Window for in Vivo Imaging. *Nature Nanotechnology* **2009,** *4* (11), 710-711.
[205] Y. Wu; J. Peng; D. Rutstrom; M. Koschan; C. Foster; C. L. Melcher, Unraveling the Critical Role of Site Occupancy of Lithium Codopants in $Lu_2sio_5:Ce^{3+}$

Single-Crystalline Scintillators. *ACS Applied Materials & Interfaces* **2019,** *11* (8), 8194-8201.
[206] F. Ren; L. Ding; H. Liu; Q. Huang; H. Zhang; L. Zhang; J. Zeng; Q. Sun; Z. Li; M. Gao, Ultra-Small Nanocluster Mediated Synthesis of Nd^{3+} -Doped Core-Shell Nanocrystals with Emission in the Second near-Infrared Window for Multimodal Imaging of Tumor Vasculature. *Biomaterials* **2018,** *175*, 30-43.
[207] B. Huang, Native Point Defects in Cas: Focus on Intrinsic Defects and Rare Earth Ion Dopant Levels for up-Converted Persistent Luminescence. *Inorganic Chemistry* **2015,** *54* (23), 11423-11440.
[208] Q. Ju; S. Luo; C. Chen; Z. Fang; S. Gao; G. Chen; X. Chen; N. Gu, Single-Irradiation Simultaneous Dual-Modal Bioimaging Using Nanostructure Scintillators as Single Contrast Agent. *Adv Healthc Mater* **2019,** *8* (9), e1801324.
[209] X. Zhong; X. Wang; G. Zhan; Y. Tang; Y. Yao; Z. Dong; L. Hou; H. Zhao; S. Zeng; J. Hu; L. Cheng; X. Yang, Nacef4:Gd,Tb Scintillator as an X-Ray Responsive Photosensitizer for Multimodal Imaging-Guided Synchronous Radio/Radiodynamic Therapy. *Nano Lett* **2019,** *19* (11), 8234-8244.
[210] M. Lowdon; P. G. Martin; M. W. J. Hubbard; M. P. Taggart; D. T. Connor; Y. Verbelen; P. J. Sellin; T. B. Scott, Evaluation of Scintillator Detection Materials for Application within Airborne Environmental Radiation Monitoring. *Sensors* **2019,** *19* (18), 3828.
[211] N. Cherepy; S. A. Payne; S. Asztalos; G. Hull; J. Kuntz; T. Niedermayr; S. Pimputkar; J. Roberts; R. D. Sanner; T. M. Tillotson; E. van Loef; C. M. Wilson; K. S. Shah; U. N. Roy; R. Hawrami; A. Burger; L. Boatner; W.-S. Choong; W. Moses, Scintillators with Potential to Supersede Lanthanum Bromide. *Nuclear Science, IEEE Transactions on* **2009,** *56*, 873-880.
[212] Q. Xu; W. Shao; J. Liu; Z. Zhu; X. Ouyang; J. Cai; B. Liu; B. Liang; Z. Wu; X. Ouyang, Bulk Organic–Inorganic Methylammonium Lead Halide Perovskite Single Crystals for Indirect Gamma Ray Detection. *ACS Applied Materials & Interfaces* **2019,** *11* (50), 47485-47490.

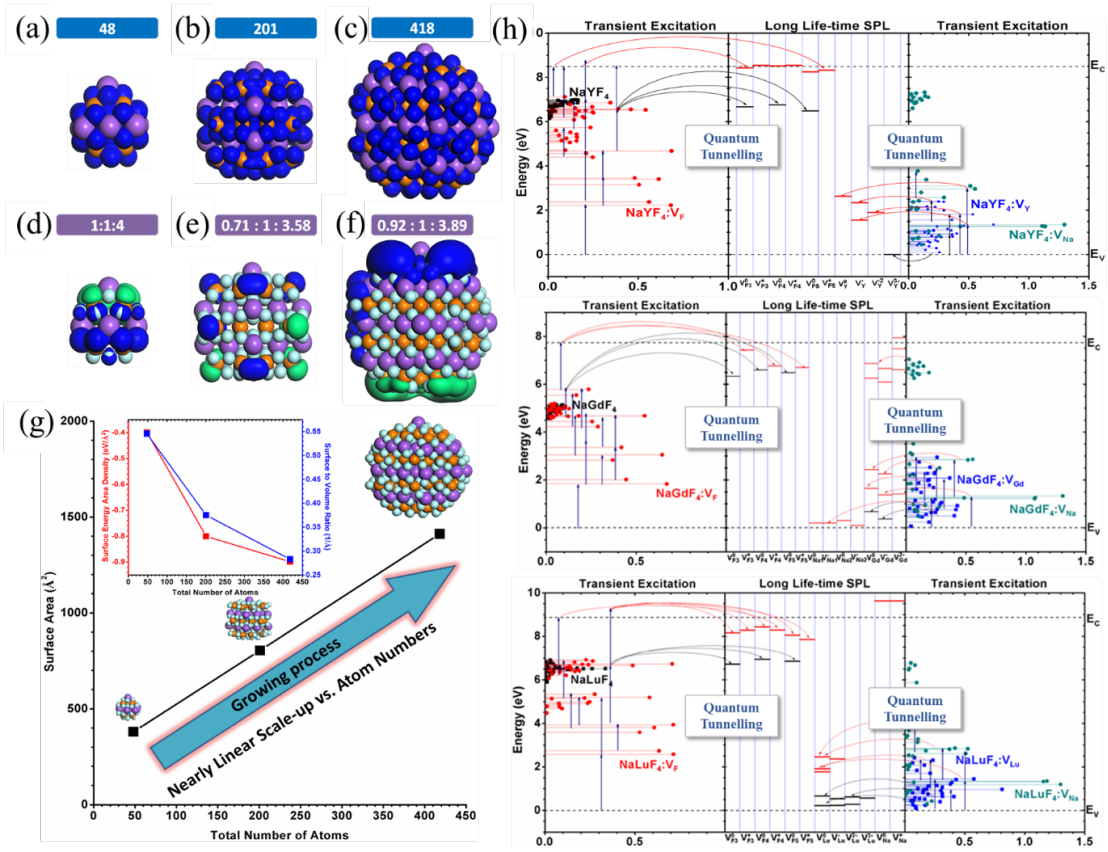

Figure 1. Electronic distribution, particle growth trends, quantum tunneling effects in energy transfer are shown for $NaYF_4$ UCNPs. a-c, The valence electronic density for different sized $NaYF_4$ nanoparticles, 48-atom, 201-atom, and 418-atom, respectively. **d-f,** Localized electronic and hole orbitals on the surface of the 48-atom, 201-atom, and 418-atom sized $NaYF_4$ respectively (Purple balls = Na, Orange balls = Y, Cyan balls = F; blue isosurfaces = electronic orbitals, green isosurfaces= hole orbitals). **g,** The surface area, surface energy area density σ_s, and surface to volume ratio with related to the size dependence. The number of atoms is the driving variable. **h**, Energy conversion, transfer, and storage via the quantum tunneling from the transient state excited electrons into the long life-time trapped electrons for $NaREF_4$ (RE=Y, Gd, and Lu). [110] Copyright 2019, Elsevier.

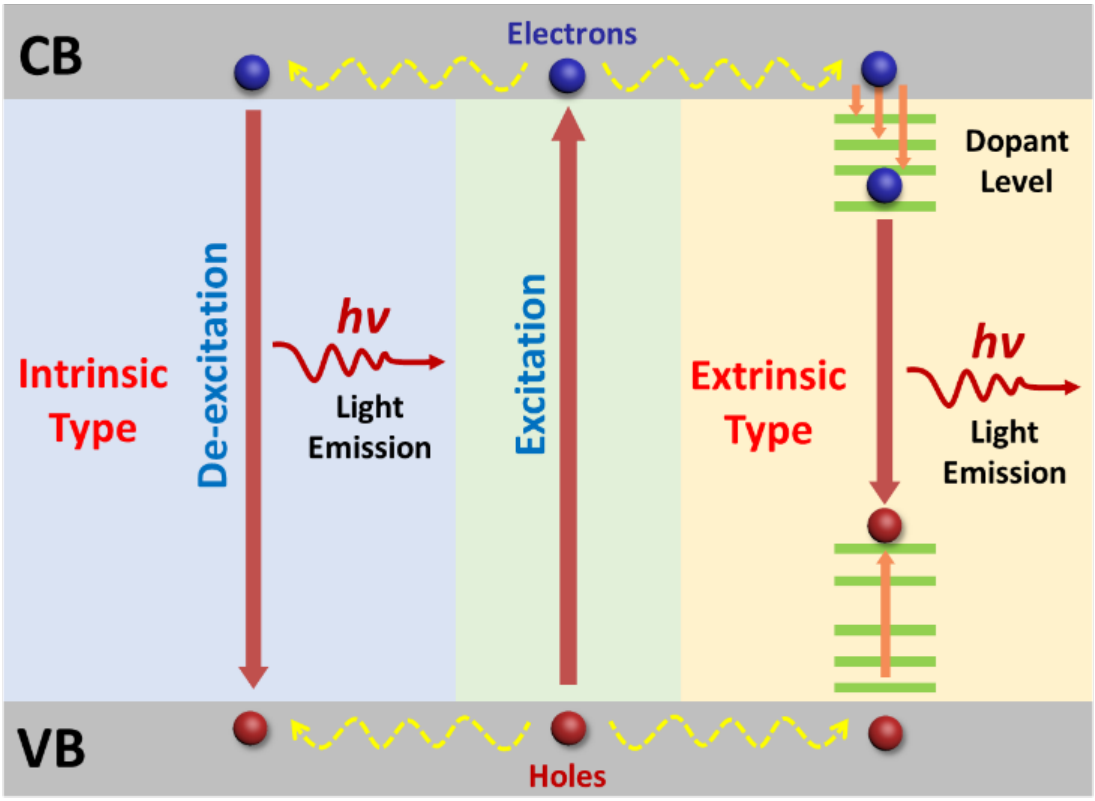

Scheme 1. Two typical mechanisms that explain the photon emission process of inorganic scintillating materials: the intrinsic type and extrinsic type.

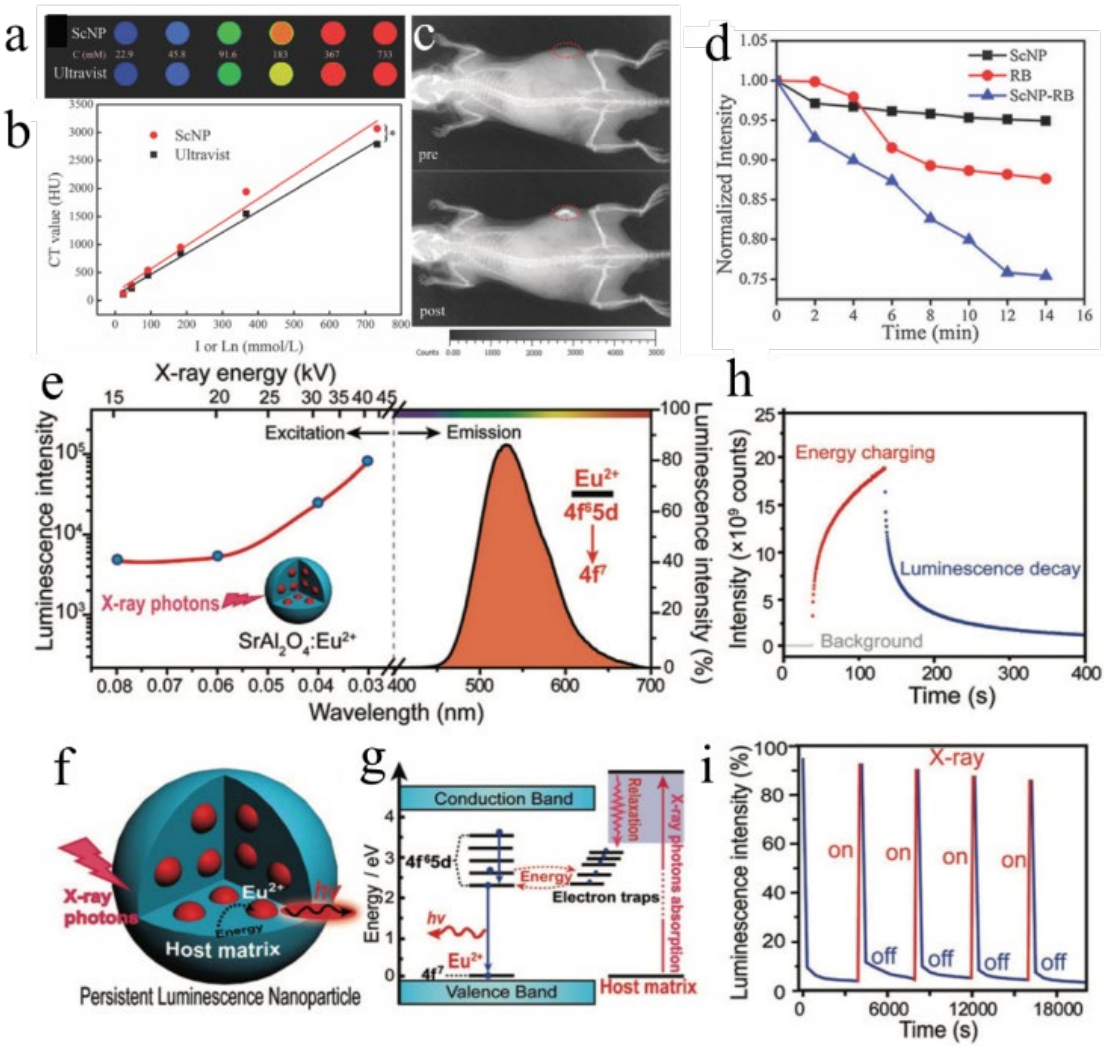

Figure 2. (a) Colored CT mapping of LaF_3: Tb^{3+}-RB ScNPs (scintillating nanoparticles) and commercial contrast medium Ultravist® 300 in various concentrations. (b) The CT values recorded by ScNPs-RB and Ultravists® 300 respectively. (c) X-ray images of cancer-bearing mice after pre- and post-intratumor injected with ScNPs-RB. (d) The decay curve of absorption at 410 nm induced by ScNPs, RB, and ScNPs-RB respectively. (a) - (d) are reprinted with permission.[144] Copyright 2015, the Royal Society of Chemistry. (e) X-ray stimulated emission spectrum of PEG-$SrAl_2O_3$: Eu^{2+} and the variation of emission intensity under different X-ray tube voltage. (f) and (g) Schematic depiction of the afterglow emission of $SrAl_2O_3$: Eu^{2+} nanoparticles. (h) X-ray charging and luminescence decay. (i) Photo-stability Testing. (e) to (i) are reprinted with permission.[146] Copyright 2017, the Royal Society of Chemistry.

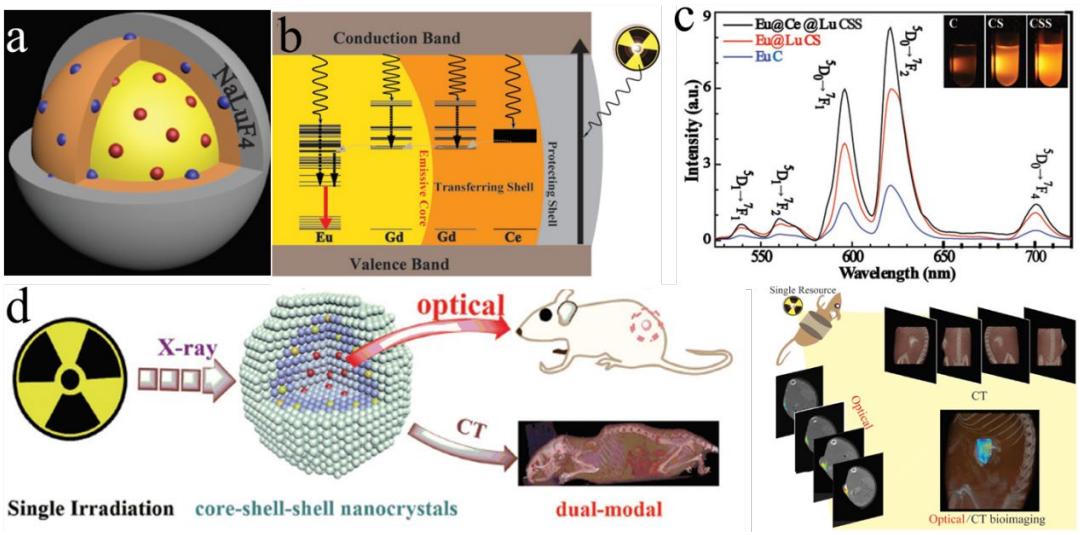

Figure 3. (a) Illustrating the spatial structure of the core-shell-shell nanocrystals. (b) Proposed energy transfer principles of the nanoparticles under X-ray radiation to realize bright light emission. (c) Comparison of X-ray activated emission spectra of core, core-shell, core-shell-shell structured nanoparticles. The inset indicates the luminous images of these three samples in aqueous solution under the X-ray radiation. (d) Schematic illustration of the dual-modal imaging platform (left). CT, optical and dual-modal images of 4T1 cancer-bearing mice after the intratumor injection of PAA-capped nanoparticles, recorded from the single-illumination dual-modal imaging platform (right).[208] Reprinted with permission. Copyright 2019, Wiley-VCH.

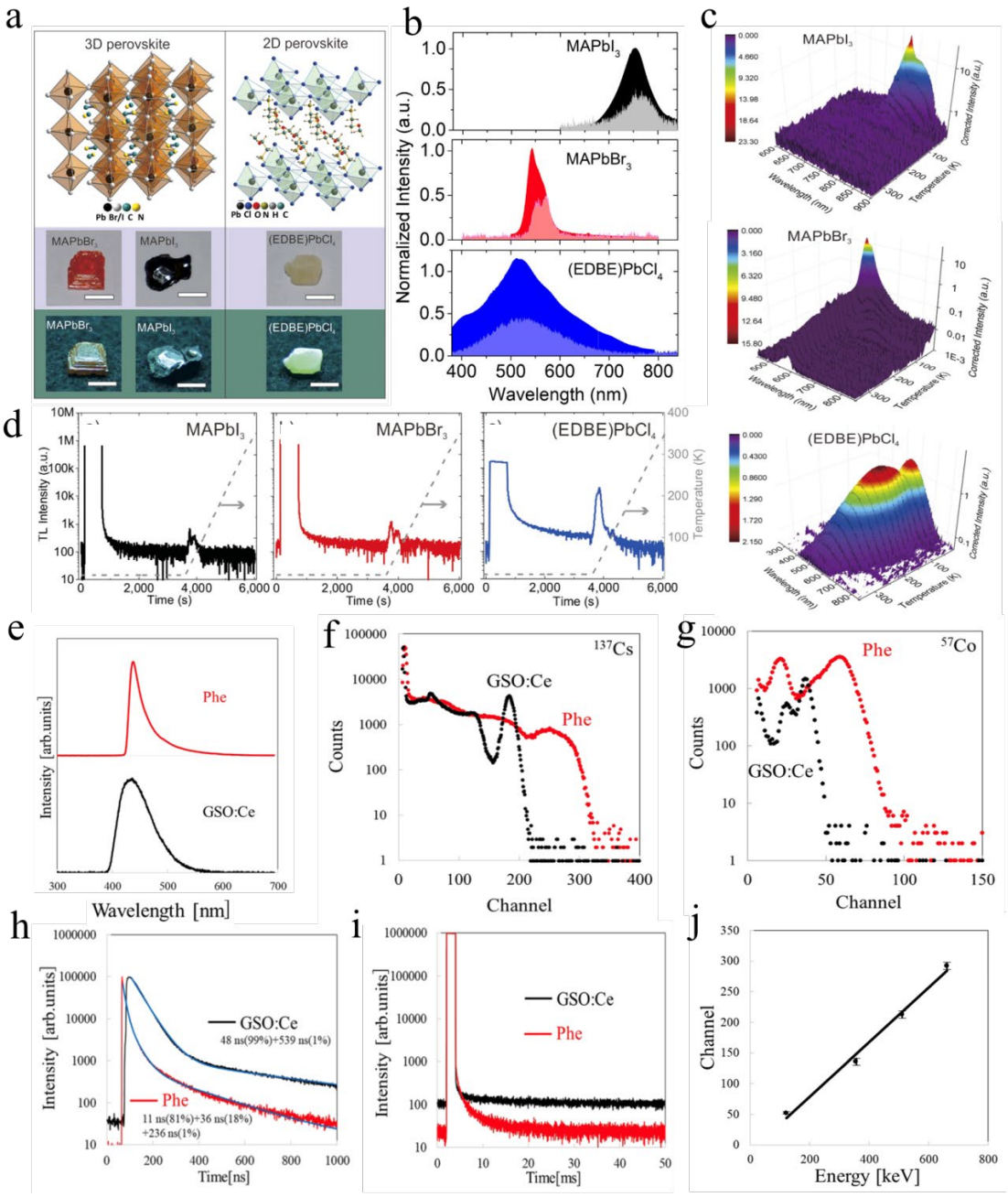

Figure 4. (a) Top: crystalline structure of $MAPbBr_3$ and $MAPbI_3$ 3D perovskites (left); EDBE-$PbCl_4$ 2D perovskite (right); middle: photos of the single-crystal hybrid Pb-halide perovskites; bottom: shining of the single-crystal hybrid perovskites under UV excitation. (b) Scintillation spectra of $MAPbI_3$, $MAPbBr_3$ and EDBE-$PbCl_4$ under X-ray (light-color region) and photo (dark-color region) excitation respectively. (c) X-ray excited scintillating spectra of $MAPbI_3$, $MAPbBr_3$, and EDBE-$PbCl_4$ perovskites at different temperatures (10 K-350 K). (d) Residual luminescence background after X-ray irradiation. Low-temperature thermal luminescence (TL) curves of $MAPbI_3$, $MAPbBr_3$, and EDBE-$PbCl_4$. The data are displayed on the time scale from 10 K and increasing to 350 K after 3600 s (the dashed line in the right panel).[23] Copyright 2016, Springer Nature Limited. (e) Emission spectra of $(C_6H_5C_2H_4NH_3)_2PbBr_4$ (Phe) and GSO: Ce under X-ray excitation. (f) ^{137}Cs and (g) ^{57}Co induced pulse height spectra of Phe and GSO: Ce respectively. (h) Scintillating decay time profile of Phe and GSO: Ce under X-ray excitation. (i) X-ray induced PL time profiles of Phe and GSO: Ce. (j)

Correlation between the pulse height channel and γ-ray energy.[83] Copyright 2017, Springer Nature Limited.

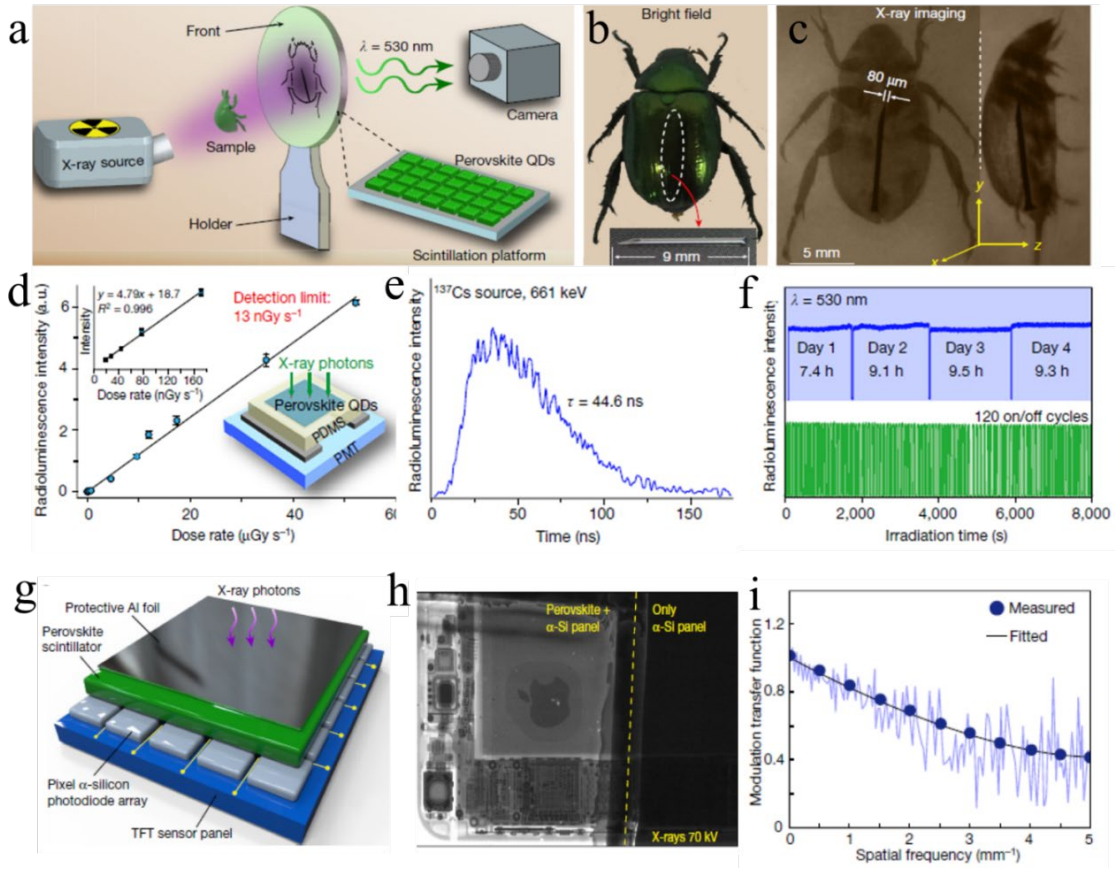

Figure 5. (a) Schematic of the experimental setup used for real-time X-ray imaging of biological samples. (b) Bright-field and the (c) X-ray images of the sample. (d) Radioluminescence measurements for a $CsPbBr_3$-based scintillator as a function of dose rate. The left inset shows radioluminescence profiles measured at low dose rates. The right inset shows a schematic of the X-ray photodetector. (e) Measured radioluminescence decay of the $CsPbBr_3$-based scintillator under excitation with a 137Cs source. (f) Photostability of the $CsPbBr_3$-based scintillator against continuous X-ray irradiation (top) and repeated cycles of X-ray excitation at 30 kV with a time interval of 30 s (bottom). (g) Multilayered design of the flat-panel X-ray imaging system consisting of a thin-film-transistor (TFT) sensor panel, a pixelated α-silicon photodiode array, a $CsPbBr_3$ perovskite nanocrystal thin-film and a protective Al foil cover. (h) Comparison of X-ray images of an Apple iPhone acquired with the perovskite scintillator deposited on an α-Si photodiode panel (left) and only with an α-Si photodiode (right) (i) Spatial resolution of the X-ray imaging system. The blue circles and purple line show measured values and the black line is a fit to the data.[7] Reprinted with permission. Copyright 2018 Springer Nature Limited.

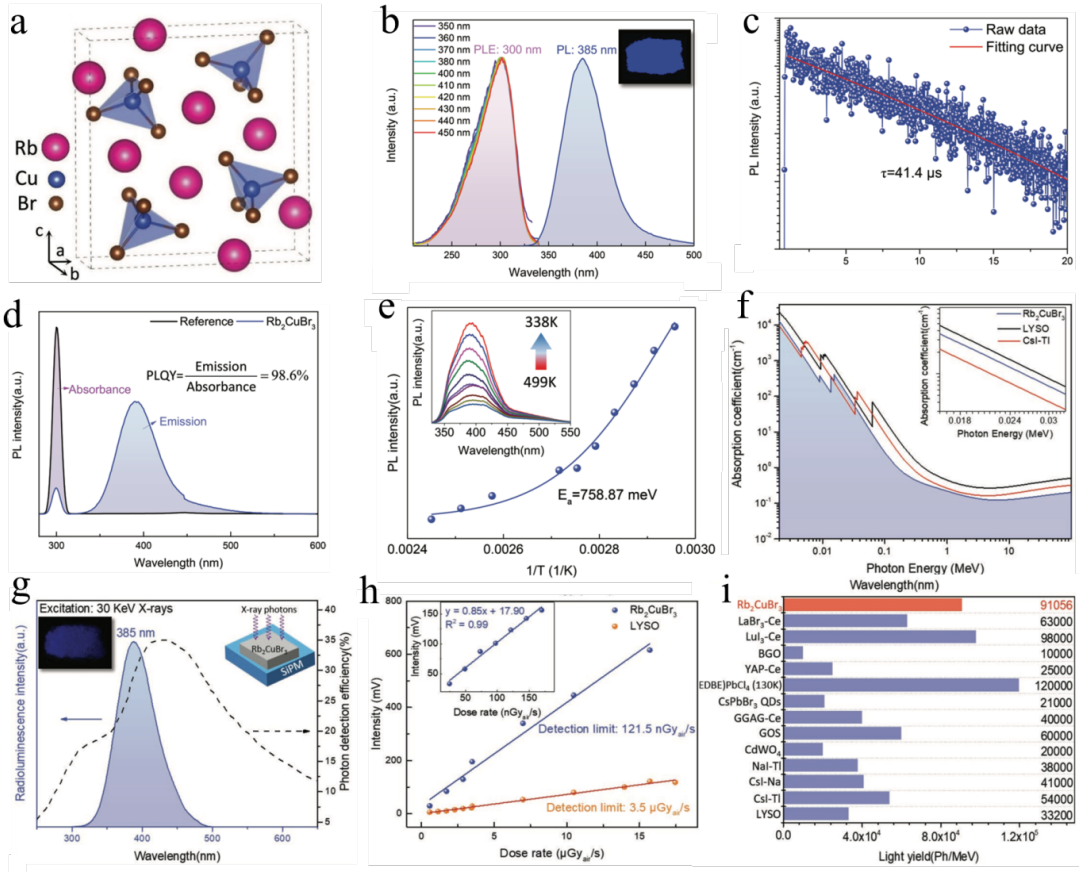

Figure 6. (a) Crystalline structure of Rb_2CuBr_3. (b) The photoluminescence spectra of Rb_2CuBr_3 under 300 nm excitation and PLE spectra obtained at various emission wavelengths (350 nm - 450 nm). The inset indicates the emission photograph under an excitation wavelength of 302 nm. (c) Time-resolved photoluminescence decay spectrum at room temperature. (d) The PLQY spectra of the Rb_2CuBr_3 scintillator. (e) Integrated photoluminescence intensity as a function of reciprocal temperature (98 K - 409 K). The inset illustrates the temperature-dependent photoluminescence spectra. (f) Absorption-coefficient values of Rb_2CuBr_3, CsI: Tl, and LYSO as the function of photon-energy from 1 keV (soft X-ray) to 100 MeV (γ-ray). (g) Radio luminescence spectrum under 30 keV X-ray irradiation and wavelength-dependent photon detection efficiency of SiPM. The left inset presents the photograph of the Rb_2CuBr_3 scintillator under X-ray excitation and the right inset presents the schematic model for detecting the emission intensity via SiPM. (h) Scintillation intensity of Rb_2CuBr_3 and LYSO as a linear function to dose rate. The inset indicates the corresponding data of Rb_2CuBr_3 measured below 200 nGy_{air}/s for the calculation of the detection limit. (i) The comparison of LY between the nontoxic Rb_2CuBr_3 and previously reported typical scintillators. Reprinted with permission. Copyright 2019, Wiley-VCH.

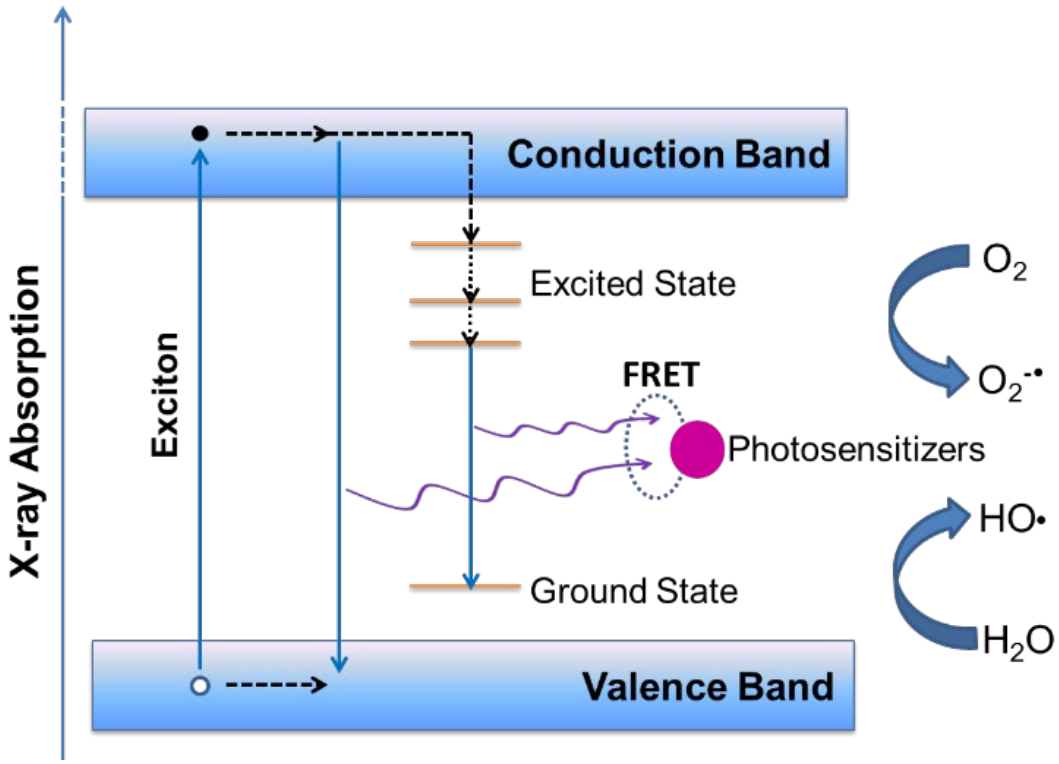

Scheme 2. The mechanism of X-ray activated NPs for PDT.

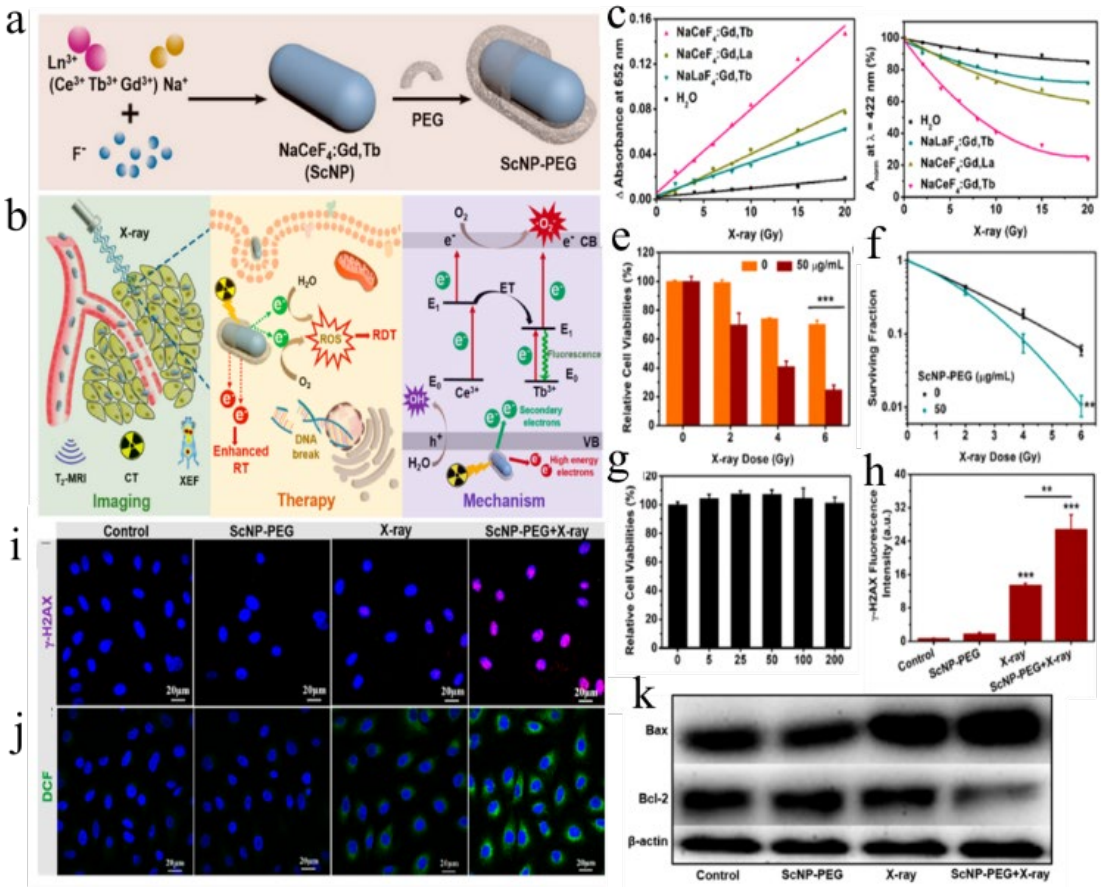

Figure 7. (a) and (b) Schematic Illustration of X-ray Activated $NaCeF_4$: Gd, Tb scintillator for XEF/CT/T2-MR Imaging-Guided Synchronous RT and RDT of Tumor. (c) and (d) $\bullet O^{2-}$ and •OH generations with ScNP-PEG under X-ray radiation detected by DPBF and TMB as trapping agents, respectively. (e) Viabilities of A549 cells treated with 50 μg mL^{-1} of ScNP-PEG under X-ray radiation. (f) The dose-effect curve of A549 cell survival detection by clonogenic assay. (g) Viabilities of A549 cells treated with different concentrations of ScNP-PEG. (h) and (i) Fluorescence images and quantification of DNA damages induced by ScNP-PEG (50 μg mL^{-1}) under X-ray radiation (6Gy), stained with γ-H2AX for DNA fragmentation visualization. (j) Fluorescence images of the cellular oxidative stress. (k) Bax and Bcl-2 expressions were analyzed by Western blot.[209] Reprinted with permission. Copyright 2019 American Chemical Society.

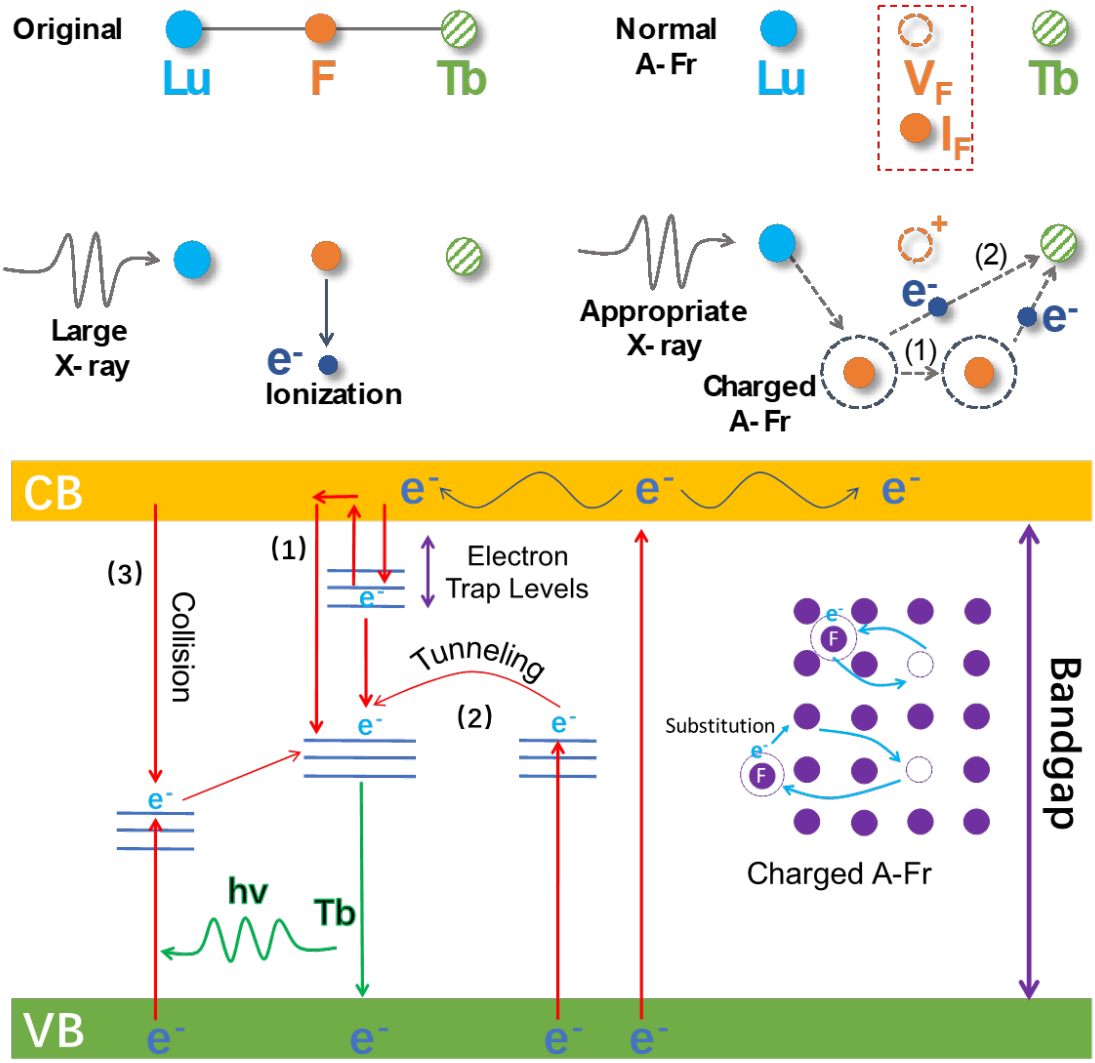

Scheme 3. The charged A-Fr defects dominated mechanism for the ultra-long emission in Tb: $NaLuF_4$.

Table 1. Summary on the key properties of scintillating materials in X-ray medical imaging.

Scintillator	Density (g/cm^3)	Peak Emission (nm)	Light Yield (ph/MeV)	Decay Time (ns)	Afterglow (% after 3 ms)	Ref
NaI(Tl)	3.67	415	38000-55000	250	-	[91, 210]
$CdWO_4$	7.9	495	28000	5000	0.05	[105, 173]
BGO	7.13	480	8000-10000	300		[91, 210]
$LaBr_3$	5.08-5.22	380	63000	12		[91, 211]
LYSO(Ce)	7.1-7.2	420	30000-33000	45		[210]
Gd_2O_2S:Tb(Ce) (GOS)	7.34	550	50000	6×10^5	0.6	[105]
Gd_2O_2S:Pr,Ce,F (GOS)	7.34	520	50000	2400	<0.1	[105]
$CsPbBr_3$	-	525	21000	8.09		[73]
$MAPbBr_xCl_{3-x}$	-	410-600	18000	0.14		[212]
2D (EDBE)$PbCl_4$	2.19	520	12000	7.9		[23]